



山西大學
Shanxi University

2022 硕士学位论文

光悬浮纳米粒子的旋转与散射光干涉研究

作者姓名 SHAH JEE RAHMAN

指导教师 张靖 教授/于旭东 副教授

学科专业 光学

研究方向 量子光学

培养单位 量子光学与光量子器件国家重点实验室

光电研究所

学习年限 2019 年 9 月至 2022 年 6 月

二〇二二年六月



山西大学
SHANXI UNIVERSITY

Thesis for Master's degree, Shanxi University, 2022

Rotation and scattered light interference of optically
levitated nanoparticles

Student Name	Shah Jee Rahman
Supervisor	Prof. Jing Zhang
Co-supervisor	Xudong Yu
Major	Optics
Specialty	Quantum Optics
Department	State Key Laboratory of Quantum Optics and Quantum Optics Devices Institute of Opto-Electronics
Research Duration	2019.09-2022.06

June, 2022

山西大学

2022 硕士学位论文

光悬浮纳米粒子的旋转与散射光干涉研究

作者姓名 SHAH JEE RAHMAN

指导教师 张靖 教授/于旭东 副教授

学科专业 光学

研究方向 量子光学

培养单位 量子光学与光量子器件国家重点实验室

光电研究所

学习年限 2019 年 9 月至 2022 年 6 月

二〇二二年六月

中文摘要

近年来，真空中光悬浮微纳米粒子引起了广泛关注，成为了精密测量和基础物理研究不可或缺的平台。光学悬浮颗粒处于自由空间，可以实现与热环境以及基片引起的退相干。并且由于高 Q 因子，而使其对周围环境的变化非常敏感，成为超精密测量高频引力波、短程力的理想候选者。最近已经实现了被捕获纳米粒子的质心运动的量子基态冷却，这可用于检验宏观量子叠加和退相干理论。此外，光场角动量的转移导致各向异性粒子以非常高的速度旋转，可用于超灵敏扭矩测量。

首先，本论文简要讨论了微纳米粒子捕获的历史，详细分析了光悬浮粒子捕获的实验原理，主要阐述三种不同的方法来计算与粒子直径(d)和激光波长(λ)相关的纳米/微球上的光场作用力。如果 $d \gg \lambda$, 则可以使用几何光学方法；如果($d \ll \lambda$), 那么瑞利散射会更合适；最后，讨论 $d \approx \lambda$ 时, 需要应用 Mie 散射方法。由高数值孔径强聚焦的激光束在焦点区域产生稳定的三维势阱，使粒子囚禁在势阱中，而对于光俘获粒子的运动，可利用朗之万方程和涨落耗散定理，研究了粒子的运动，以及阻尼率与压力的关系，并进一步讨论了的质心运动冷却的实现方法。

其次，描述了光学悬浮纳米粒子系统的基本结构与实验方法。实验上，我们利用 1064nm 激光进行捕获，同时探测捕获光束与散射光，来检测纳米粒子的质心运动、扭转和旋转信号。为此，设计了一个套的真空系统，包括：真空室、真空阀、真空管、电极、真空计和真空泵。考虑到高真空环境下捕获的稳定性，我们选择球形二氧化硅纳米颗粒作为研究对象。针对光悬浮系统中粒子质心运动信号微弱的特点，采用平衡探测方法对粒子在轴向和径向的运动信号进行检测。以 x 方向为例对数据记录和分析进行了概述。

然后，实验研究了在不施加反馈冷却的情况下，采用竖直光路设计和利用高数值孔径物镜对单个纳米粒子的捕获。当捕获激光为线偏振时，我们测量了粒子质心运动，并测量粒子的扭转运动。通过将捕获光的线偏振改变为圆偏振，我们用利高速光纤探测器检测到纳米粒子的高速旋转频率（4.9 GHz），高速机械转子可用于极端情况下材料特性检测与真空摩擦的相关研究。

最后，我们利用散射成像研究了在单个势阱中光学悬浮的两个二氧化硅纳米粒子散射光的干涉，真空悬浮提供了一个无粒子-基片相互作用的环境。实验中，我们使用两束指向有微小差别的 1064 nm 激光束捕获两个纳米粒子。其中一束 1064 nm 激光由马达驱动的反射镜精确控制，使两势阱重叠，然后将两个粒子囚禁在单个势

阱中。另一束线偏振 532 nm 激光垂直于捕获激光束的方向照射两个纳米粒子，两个纳米粒子的散射光由同一物镜收集，在 CCD 上成像。通过旋转捕获光束偏振和照明光束偏振，在像空间和傅立叶空间（ k 空间）中测量散射光的干涉。该系统可用于悬浮粒子动力学特性、散射各向异性、近场光学以及成像领域的相关研究。

关键词： 辐射压力； 光镊； 悬浮； 质心运动； 扭转和旋转运动；
散射光干涉.

Abstract

In recent years, optically levitated micro-nanoparticles in vacuum have attracted widespread attention, and have become an indispensable platform for precise measurement and fundamental physics research. Optical levitation eliminates the need to fetter the particle, and excellent decoupling can be achieved from the thermal environment and decoherence caused by a substrate. Because of its high Q factor in vacuum, it is very sensitive to changes in the surrounding environment, making it an ideal candidate for ultra-precise measurement of high-frequency gravitational waves and short-range forces. More recently, it has been realized to cool the center-of-mass motion of optically trapped nanoparticles to reach the quantum ground state, which can be used to test the theory of macroscopic quantum superposition and decoherence. Furthermore, the transfer of the angular momentum of the light field causes anisotropic particles to rotate at very high speeds, and can be used to measure ultra-sensitive torques.

In the first chapter of this dissertation, we briefly discuss the history of trapped micro-nanoparticle, analyzes the experimental principle of optically levitated particles in detail, and mainly uses three different methods to calculate the light field force on the nano/microspheres related to particle diameter (d) and laser wavelength (λ). If ($d \gg \lambda$), then ray optics can be utilized; if ($d \ll \lambda$), then Rayleigh scattering will be more appropriate; and finally, if ($d \approx \lambda$), we may need to use the Mie scattering approach. A laser beam intensely focused by a high numerical aperture objective lens generates a stable three-dimensional potential well at the focal region, and traps the particles within it. The Langevin's equation and the fluctuation dissipation theorem can be used to study the motion of the particles as well as the relationship between the damping rate and the pressure, which also explains the realization method of center-of-mass motion cooling.

Secondly, the basic optical setup and experimental components of the optically levitated nanoparticle system are described in details. In the experiment, we use a 1064 nm laser for trapping, and simultaneously collect the scattered and trapping beam's output light to detect the nanoparticle's center-of-mass motion signal, torsional signal, and rotation signal. For this purpose, we designed a complete vacuum system that includes a vacuum chamber, vacuum valves, vacuum pipes, vacuum electrodes, vacuum gauges, and

vacuum pumps. We chose spherical silica nano-particles as a research object for our experiments by considering the stability of trapping under high vacuum. Keeping in view, the weak signal of particle's center-of-mass motion in the optically levitated system, a balanced homodyne detection method is used to detect the motion signal of particles in the axial and radial directions. An overview of data recording and analysis is given with an example of x-direction analysis.

Furthermore, the experiment investigates the use of vertical optical path design and utilizes a high numerical aperture objective lens to trap an individual nanoparticle without applying feedback cooling. When the trapping laser beam is linearly polarized, we measure the center-of-mass motion and torsional motion of the nanoparticle. By changing the linear polarization of the trapping beam to circular polarization, we detect a very high-speed rotation frequency (4.9 GHz) of the nanoparticle with a high-speed fiber detector. The high-speed mechanical rotor can be used for material characteristic detection and vacuum friction under extreme conditions.

Finally, we use scattered light imaging to study the interference of light scattered by two silica nanoparticles optically levitated in a single potential well, as levitation in vacuum provides an environment free of particle-substrate interactions. We use two beams of 1064 nm laser with slight differences in pointing to trap two nanoparticles. One of the 1064 nm laser beams is precisely controlled by a motor-driving mirror to overlap the two potential wells and trap two nanoparticles in a single potential well. Another linearly polarized 532 nm laser beam illuminates the two nanoparticles perpendicular to the direction of the trapping laser beam, and scattered light of the two nanoparticles is collected by the same objective lens and imaged on a CCD. The interference of scattered light is measured in image and Fourier space (k-space) by rotating the trapping beam polarization and illuminating beam polarization. This system can be used to study the dynamical properties, scattering anisotropy, near-field optics, optical trapping, and imaging.

Key words: Radiation pressure; Optical tweezers; Levitation; Centre-of-mass motion; Torsional and rotation motion; Scattered light interference

Contents

中文摘要.....	IV
Abstract	VI
Chapter 1: Introduction	1
1.1 History of Nano- and Micro-sphere trapping	1
1.2 Radiation pressure on a mirror	2
1.3 Theories for calculating the radiation force.....	3
1.3.1 Ray optics approximation.....	4
1.3.2 Rayleigh scattering approximation.....	5
1.3.3 Lorentz-Mie scattering theory	7
1.4 Summary	8
Chapter 2: Optically levitated nanoparticle’s motion and application	10
2.1 CoM motion of nanoparticles.....	10
2.1.1 Motion of optically trapped nanoparticles.....	10
2.1.2 Damping rate of CoM motion	11
2.2 Cooling the CoM motion of nanoparticles	12
2.2.1 Active feedback cooling.....	13
2.2.2 Parametric feedback cooling	14
2.2.3 Electric feedback cooling	15
2.2.4 Cavity cooling	16
2.3 Applications of optically trapped nanoparticles.	16
2.4 Summary	16
Chapter 3: Experimental setup for optically levitated nanoparticles	18
3.1 Introduction	18
3.2 Optical path and essential components.....	19
3.3 Vacuum system	20
3.4 Selection of particles and loading.....	23
3.4.1 Making solution.....	24
3.4.2 Loading of nanoparticles	25
3.5 Detection system	26

3.5.1 Radial detection	27
3.5.2 Axial detection	29
3.5.3 Balanced homodyne detector	30
3.6 Data recording and analysis	32
3.6.1 Data analysis.....	32
3.7 Summary	34
Chapter 4: Rotational Optomechanics	37
4.1 Introduction	37
4.2 Optically levitated nanoparticles motion.....	37
4.3 Experimental observation of nanoparticle’s rotation.....	38
4.3.1 Experimental setup	38
4.3.2 CoM motion and torsional vibration measurement	40
4.3.3 Rotational motion without feedback cooling system	41
4.4 Conclusion.....	43
Chapter 5: Interference of the scattered light from two optically levitated nanoparticles.....	44
5.1 Introduction	44
5.2 Theoretical explanation	46
5.3 Experiment	48
5.4 Results and discussion.....	51
5.5 Summary	54
References	55
Research achievements	64
Acknowledgments.....	65
Personal Profile	67
Letter of commitment	68
Authorization statement	69

Chapter 1: Introduction

1.1 History of Nano- and Micro-sphere trapping

During 1619, Johannes Kepler proposed that a comet's tail all the time pointing away from the Sun could be explained with the help of radiated light from the Sun^[1]. About 250 years later, in 1873, James C. Maxwell figured out the mathematical framework for magnetism and electricity. He concluded from his theoretical derivations that electromagnetic radiation has momentum^[2]. In 1900, this idea was shown by Pyotr Lebedev experimentally^[3] and in 1901, by Ernest F. Nichols and G. F. Hull^[4]. At that time, this was quite exciting, but very little progress was made until the invention of lasers by Charles Townes in 1960^[5].

Lasers have numerous uses and play an important role in physics, chemistry, and biology. One of the most important uses of lasers is trapping particles through optical tweezers. Optical tweezers are generally an optical technology that uses the radiation pressure (force per unit area on an object due to change in light momentum) of the light field at the focal point of an intensely focused laser to capture and manipulate tiny-scale spherical particles or asymmetric particles. Undoubtedly, we can say Arthur Ashkin is the father of bead trapping. On 26th January 1970, Ashkin trapped and accelerated a micron-sized particle in a stable potential well utilizing the radiation pressure from a CW visible laser (514.5 nm) while working in Bell Telephone Laboratories, Holmdel, New Jersey. He performed experiments in liquids and air. In his work, Ashkin differentiated two components of radiation pressure. The first referred to the force due to the scattering of light directed along the laser propagation axis. At the same time, the second one referred to gradient force that is in the direction of the intensity gradient of the laser field. Arthur Ashkin won the 2018 Noble Prize in Physics for optical tweezers technology^[6]. On 15th October 1971, A. Ashkin and J. M. Dziedzic published another paper in which they stably trapped a transparent glass micro-sphere (20 μm) by radiation pressure in air and vacuum at pressure down to ~ 1 Torr^[7]. In 1975, A. Ashkin and J. M. Dziedzic trapped oil droplets down to $\sim 10^{-6}$ Torr, a high vacuum regime. This work discussed radiometric forces

arising from temperature gradients around the sphere that destabilize the trapped sphere^[8]. In 1976, A. Ashkin and J. M. Dziedzic published another paper that addresses a feedback cooling technique for stabilizing glass microsphere in vacuum and air, and preventing the particles loss from the optical trap in low pressure around 1 Torr due to radiometric forces^[9].

During 1987, Ashkin used optical tweezers to capture a single tobacco mosaic virus successfully, and dense oriented arrays of viruses were also trapped in a liquid solution without affecting their activity with a 120 mW power of argon laser. He also demonstrated the trapping of single live, *motile* bacteria *E-coli* without harming their activities at a few milliwatts of power^[10]. This was a significant breakthrough in the developmental history of optical tweezers. Even though the exact theory for optical tweezers is still to be developed and mostly the theories are approximations based, the basic principles for trapping particles with a much larger or smaller diameter (size) than the wavelength of laser light are very straightforward. The electric field of the incident light develops an electric dipole moment in small objects, which brings up an intensity gradient in the electric field toward the central focus point. On the other hand, larger transparent objects act like lenses, the light gets refracted, and the photon's momentum redirects. The recoil of photons pushes the particles toward the higher flux of photons near the point of focus^[11, 12].

1.2 Radiation pressure on a mirror

Arthur Ashkin proposed the first-ever calculation of radiation pressure in his seminal paper on radiation pressure^[6]. It can be defined as the force per unit area on an object due to a change in light momentum.

However, radiation forces are weak, and only high-power focused laser beams can levitate tiny objects- up to 30 μm in size^[13].

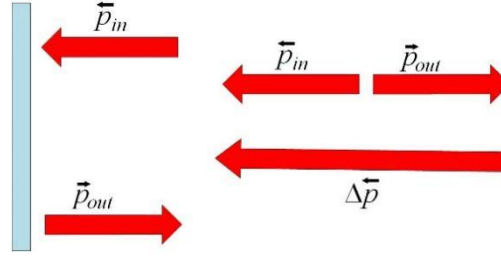


Figure 1.1. Illustration of the change in momentum from a 0° reflecting mirror, incident, and reflected momentum.

Figure 1.1 shows the reflection of a single photon from the mirror and its momentum change. The magnitude of the photon's momentum before and after reflection can be written as $p = \frac{h\nu}{c}$; where p represents momentum, ν is the photon's frequency, h is Plank's constant, and c is the speed of light. After the total reflection change in momentum is:

$$|\vec{p}_{in} - \vec{p}_{out}| = 2p = 2\frac{h\nu}{c} \quad (1.1)$$

Now, let's suppose we use a laser source of power P on the exact mirror instead of a single photon. Photon striking the mirror per second is $\frac{P}{h\nu}$ and will have radiation force $F_{radiation}$ on the mirror, which is given by:

$$F_{radiation} = \frac{\Delta p}{\Delta t} = 2\frac{h\nu}{c} \frac{P}{h\nu} = \frac{2P}{c} \quad (1.2)$$

For $P = 2W$,

$$F_{radiation} = \frac{2 \times 2W}{3 \times 10^8 \text{ m/s}} = 1.33nN \quad (1.3)$$

This force is significantly small and can only levitate and accelerate particles with smaller masses.

1.3 Theories for calculating the radiation force

Mainly three different theories are used to calculate the force on a Nano/microsphere related to the bead diameter (d) and laser wavelength (λ). If the diameter of the bead is much larger than the wavelength of the laser ($d \gg \lambda$), then ray optics can be utilized. If the bead diameter is much smaller than laser wavelength ($d \ll \lambda$), then Rayleigh scattering will be more appropriate. Finally, if the bead diameter and wavelength are comparable ($d \approx \lambda$), we may need to use the Mie scattering approach.

1.3.1 Ray optics approximation

In 1687, sir Isaac Newton proposed the 3rd law of motion, which states that “for every action, there is an equal and opposite reaction”. Let suppose we trap a transparent particle in the optical beam’s focal point and if the particle deviates from its focus point to aside, a large number of photons will be refracted to that side. As a result, the recoil of the photon will push the particle back to its focus point (Figure 1.2).

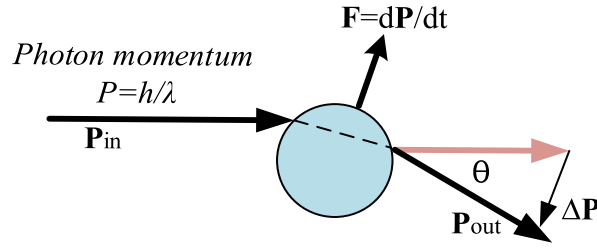


Figure 1.2. Change in photon momentum causes a force in the opposite direction.

When the size (d) of the trapped particle is much larger than the wavelength (λ) of the trapping beam, then the most appropriate theory to explain the trapped micro or nanoparticle is ray optics^[11, 14]. In Figure 1.3. (A), we have considered a particle trapped at the beam's focus with a larger diameter than the wavelength of the trapping beam, and the surface reflection from the sphere is neglected. The beam's incident and refracted photons have almost the same angle resulting in zero change in the momentum. Thus, the net force on the particle is equal or zero, and the particle is trapped stably. In Figure 1.3. (B), the sphere slightly moved in the z -direction, or we can say, in the direction of the trapping beam. The beam will be more intensely focused and increase the photon's momentum in the z -direction. The recoil force from the photons will push the particle back to the high-intensity region and vice versa. Figure 1.3. (C) shows that the particle has moved in the radial direction, and the number of deflected photons have increased in the same direction. Thus, the counterforce will push the particle back to the opposite side.

The Refractive index of the particle and medium plays a key role in trapping because the surface reflection of the particle depends upon the relative refractive index $m = n_p / n_{md}$, where n_p and n_{md} are the refractive indexes of particle and medium, respectively. If m is larger, it will be challenging to trap the particle in an optical tweezer^[15]. The Refractive index of silica is about 1.46, for air is 1, and while for water is 1.33. m is approximately

1.10 for silica in water, and in the air, it is 1.46, which shows that trapping the silica particles in the air is much more complicated than water.

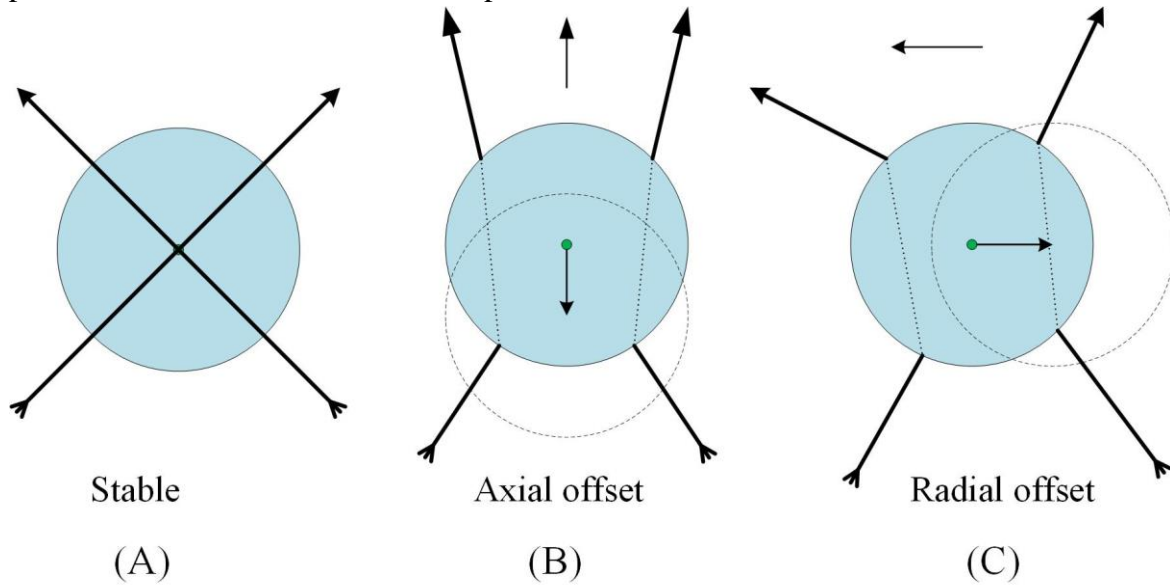


Figure 1.3. Qualitative representation of ray optics. (A) the particle is stably trapped at the focus, (B) downward or upward force. When the particle is away from the focus in z or in the direction of the trapping beam, (C) the force on the particle if the particle is off focus in xy directions.

1.3.2 Rayleigh scattering approximation

If the size of the particle is significantly smaller than the wavelength of the trapping laser beam ($d \ll \lambda$), then we can consider the nanoparticle as a dipole. Rayleigh scattering theory provides an analytical method to calculate the optical force on nanoparticles [14, 16]. The theory presented here has been obtained from Harada and Asakura (1996) [16] to calculate the radiation force in the Rayleigh regime acting on a dielectric nanoparticle. The basic diagram is given in Figure 1.4. The Gaussian beam is linearly polarized and has TEM_{00} mode. The focused laser beam has a minimum waist of ω_0 in the $(x,y,z) = (0,0,0)$ coordinates. The laser propagates along the z -axis while the polarization of the laser's electric field is along the x -axis. The dielectric nanoparticle of radius "R" is located at a distance "r" from the centre of the laser beam.

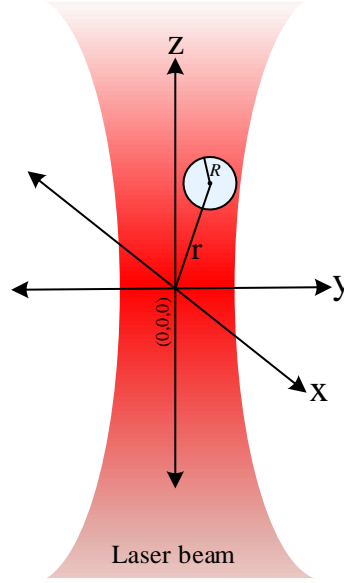


Figure 1.4. Schematic diagram of nanoparticle in the Gaussian beam (TEM_{00} mode) near the focus.

The refractive of the particle is n_p . The waist of the beam along z is given by:

$$\omega(z) = \omega_0 \left[1 + \left(\frac{\lambda_z}{\pi \omega_0^2} \right)^2 \right]^{1/2} \quad (1.4)$$

where λ is the laser wavelength, ω_0 is the least waist of the beam at $z = 0$. The intensity of the Gaussian laser beam is given by:

$$I(x, y, z) = I_0(z) e^{-\frac{2(x^2+y^2)}{\omega(z)^2}} = \frac{2P}{\pi \omega^2(z)} e^{-\frac{2(x^2+y^2)}{\omega(z)^2}} \quad (1.5)$$

In the above equation, P is the power of the laser, and $I_0(z)$ is the intensity of the laser beam at the centre. The radiation forces are of two types; one force is along the beam's propagation direction called scattering force (F_{scat}), and the other is directed towards the intensity gradient of the beam called gradient force (F_{grad}). The scattering force pushes away the particle from the focus point while the gradient force brings back the particle into the focus point of the beam intensity. Generally, the gradient force should overcome the scattering force to trap a particle stably.

F_{scat} is given below:

$$\vec{F}_{scat} = \left(\frac{n_{md}}{c} \right) C_{scat} I(x, y, z) \hat{z} = \frac{128\pi^5 R^6}{3c\lambda^4} \left(\frac{m^2 - 1}{m^2 + 2} \right) n_{md}^5 I(x, y, z) \hat{z} \quad (1.6)$$

and F_{grad} is given by

$$\vec{F}_{grad} = -\frac{2\pi n_{md} R^3}{c} \left(\frac{m^2 - 1}{m^2 + 2} \right) \nabla I(x, y, z); \quad (1.7)$$

Where n_{md} is the refractive index of the medium in which the particle is levitated, C_{scat} quantifies sphere scattering cross-section, m is the ratio of particle and medium refractive indexes.

The net force on the particle will be $\vec{F}_{net} = \vec{F}_{scat} + \vec{F}_{grad}$. The minimum scattering force along z must be negative for a stable trap. If the force is positive, the particle will be pushed forward, and it will not be possible to trap the particle stably. The size of the particle also plays an important role. Smaller particles are easy to trap because the scattering force is proportional to R^6 , and gradient force is proportional to R^3 . The scattering force decreases significantly compared to the gradient force if the size of the particle decreases.

1.3.3 Lorentz-Mie scattering theory

When the size of the particle is approximately equal to the wavelength of the laser beam ($d \approx \lambda$) in an optical tweezer, it cannot be explained with ray optics or the Rayleigh approximation. The most appropriate theory will be electromagnetic theory. If the particles are isotropic and homogeneous, then generalized Lorentz-Mie theory can explain it very well. The overall mathematical computation is very complex and excluded from this work. Here we will present an insight into the method developed by T. A. Nieminen *et al.* [17]. For the spherical particles, numerous codes have been written on Mie scattering of electromagnetic waves^[18-21].

Changes in the photon's momentum exert an optical force on the particle. Optical force on the particle can be calculated by considering the change in momentum of the photons scattered by the particle. The coordinate system to explain the light scattered by trapped particles should be a spherical coordinate system (r, θ, ϕ) . Both the fields (incoming and outgoing) can be expanded into vector spherical wave functions (In and Out)^[17]:

$$\mathbf{E}_{in} = \sum_{i=1}^{\infty} \sum_{j=-1}^i a_{ij} \mathbf{M}_{ij}^{(2)}(k\mathbf{r}) + b_{ij} \mathbf{N}_{ij}^{(2)}(k\mathbf{r}), \quad (1.8)$$

$$\mathbf{E}_{out} = \sum_{i=1}^{\infty} \sum_{j=-1}^i p_{ij} \mathbf{M}_{ij}^{(1)}(k\mathbf{r}) + q_{ij} \mathbf{N}_{ij}^{(1)}(k\mathbf{r}), \quad (1.9)$$

where $\mathbf{M}_{ij}^{(2)}(k\mathbf{r}), \mathbf{N}_{ij}^{(2)}(k\mathbf{r})$ corresponds to inward-propagating multipole fields and $\mathbf{M}_{ij}^{(1)}(k\mathbf{r}), \mathbf{N}_{ij}^{(1)}(k\mathbf{r})$ are corresponding to outward TE and TM multipole fields.

In the axial direction, optical force on the particle is given by^[17]:

$$F_z = \frac{2n_{md}P}{cS} \sum_{i=1}^{\infty} \sum_{j=-1}^i \frac{j}{i(i+1)} \operatorname{Re}(a_{ij}^* b_{ij} - p_{ij}^* q_{ij}) - \frac{1}{i+1} \left[\frac{i(1+2)(i-j+1)(i+j+1)}{(2i+1)(2i+3)} \right]^{\frac{1}{2}} \times \operatorname{Re}(a_{ij} a_{i+1,j}^* + b_{ij} b_{i+1,j}^* - p_{ij} p_{i+1,j}^* - q_{ij} q_{i+1,j}^*), \quad (1.10)$$

Where n_{md} is the medium refractive index, P is laser beam power, and c is the speed of light in space.

The normalized torque along the z -axis acting on the particle is

$$\tau_z = \frac{P}{\omega} \sum_{i=1}^{\infty} \sum_{j=-1}^i j (|a_{ij}|^2 + |b_{ij}|^2 - |p_{ij}|^2 - |q_{ij}|^2) / S \quad (1.11)$$

in units of \hbar /photon, where:

$$S = \sum_{i=1}^{\infty} \sum_{j=-1}^i (|a_{ij}|^2 + |b_{ij}|^2). \quad (1.12)$$

We can use equation (1.10) to calculate the force on particles in different environments like liquids and air. The Refractive index also plays a vital role in trapping a particle. If the refractive index of the medium is smaller, the required trapping force will also be smaller and vice versa. Higher refractive index means a higher scattering force, which results in less probability of trapping particles.

1.4 Summary

In this chapter, we have discussed a brief history of nano and microsphere trapping—the basic mathematics explaining the radiation force on a particle. When a photon hits the particle and gets scattered in a direction, a change in momentum of reflected/refracted photons occurs, which produces a recoil force. Hence, it pushes the particles in the opposite direction.

Chapter 1: Introduction

Different theories have been discussed here to calculate the radiation force on a particle depending upon the particle's size and the laser's wavelength. When the size of the particles is much bigger than the size of the laser wavelength, one has to consider ray optics. When the size of the particle is significantly smaller than the wavelength of the laser, in this case, the most appropriate theory to calculate the radiation force is the Rayleigh scattering approximation. And finally, when the size of the particle is comparable to the size of the laser wavelength, then the radiation force has to be calculated by Mie scattering approximation. In the Rayleigh scattering approximation, we saw from the calculation that the scattering force is proportional to R^6 , and the gradient force is proportional to R^3 . So, the scattering force decreases more rapidly than the gradient force, and it is easier to trap smaller particles because the negative gradient force can be achieved very quickly.

Chapter 2: Optically levitated nanoparticle's motion and application

2.1 CoM motion of nanoparticles

Brownian motion is the zigzag (random) motion of tiny particles in liquid or gas. This phenomenon was discovered in 1827 by Robert Brown^[22] while studying the movement of pollen grain particles placed in fluids with the help of a simple microscope. In 1905, Albert. Einstein published a paper in which he explained the Brownian motion correctly^[23]. The instantaneous velocity and trajectory of a Brownian particle were used to be considered not differentiable due to the reason that this was never measured successfully before. In 2010, Dr Toncang Li performed experiments using a dual-beam optical tweezer to trap the micron size particle and measured the instantaneous velocity of Brownian motion in air at different pressures^[24].

2.1.1 Motion of optically trapped nanoparticles

For simplicity, we will consider the motion of a particle's centre-of-mass in the one-dimension, i.e. only x -direction. According to the Langevin equation^[25-27], the equation of motion for a Brownian particle can be described by:

$$\ddot{x}(t) + \gamma\dot{x}(t) + \omega_0^2x(t) = \frac{F_{th}(t)}{m} \quad (2.1)$$

Where m represents the mass of levitated particles in the fluid, ω_0 is particle frequency in the x -direction. And $\gamma = 6\pi\eta R$ is the damping rate of particle's motion, R is the radius of the particle, η is the viscosity of the fluid.

$$F_{th}(t) = (2k_B T \gamma)^{1/2} \alpha(t) \quad (2.2)$$

equation (2.2) is the Brownian stochastic force, $\alpha(t)$ is the process of normalized white-noise and satisfies over t and t' .

$$\langle \alpha(t) \rangle = 0, \langle \alpha(t)\alpha(t') \rangle = \delta(t - t') \quad (2.3)$$

The power spectrum of the particle's motion signal contains information about the optical trapping levitated particle system; the Fourier transform of equation (2.1) can be obtained from Ref^[28]. By taking the Fourier transform of $x(t)$ and $\alpha(t)$:

$$X(\omega) = \int_{-\infty}^{+\infty} x(t)e^{-i\omega t} dt \quad (2.4)$$

$$A(\omega) = \int_{-\infty}^{+\infty} \alpha(t)e^{-i\omega t} dt \quad (2.5)$$

transforming equation (2.1) into Fourier:

$$-\omega^2 X(\omega) - i\omega\gamma X(\omega) + \omega_0 X(\omega) = \sqrt{\frac{2k_B T \gamma}{m}} A(\omega) \quad (2.6)$$

while

$$X(\omega) = \sqrt{\frac{2k_B T \gamma}{m}} A(\omega) \frac{1}{-\omega^2 - i\omega\gamma + \omega_0^2} \quad (2.7)$$

from equation (2.3), we can get:

$$\langle X(\omega) \rangle = 0, \langle A(\omega)^* A(\omega') \rangle = \delta(\omega - \omega') \quad (2.8)$$

then the power spectral density will be:

$$S_x(\omega) = \frac{2k_B T}{m} \frac{\gamma}{(\omega_0^2 - \omega^2)^2 + \omega^2 \gamma^2} \quad (2.9)$$

We can obtain the power spectral signal of a particle's motion according to equation (2.9), and it gives us most of the physical information about a particle.

2.1.2 Damping rate of CoM motion

In the air or vacuum environment, the damping rate of a particle's motion is related to the thermal motion of air molecules. Assuming that air particles are evenly distributed and reflection from the particle surface is diffusive, the collision between the thermal motion of air molecules and the particle is elastic. The damping rate can be calculated according to kinetic theory^[29]:

$$\gamma = \frac{6\pi\eta R}{m} \frac{0.619}{0.619 + Kn} (1 + c_k) \quad (2.10)$$

Where η is air viscosity coefficient, R is the particle's radius, m is mass of the particle, $Kn=l/R$ represents the Knudsen number, which shows the ratio of particle's free path to the particle's radius. Where c_k is a function of Kn ^[29]:

$$c_k = \frac{0.31Kn}{0.785 + 1.152Kn + Kn^2} \quad (2.11)$$

When the air pressure is very low $Kn \gg 1$, by taking the first-order approximation of the Taylor expansion for equation (2.10), we can get:

$$\gamma = 0.619 \frac{9\pi\eta d^2}{\sqrt{2}\rho k_B T} \frac{p}{r} \quad (2.12)$$

Where d represents the average diameter of air molecule, ρ is the particle's density, p is air pressure. We can see from equation (2.12) that the damping rate is proportional to air pressure. At very high pressure $Kn \ll 1$, the damping rate can be simplified as predicted by Stoke's Law.

$$\gamma = \frac{6\pi\eta r}{m} \quad (2.13)$$

We can easily determine the particle's size, temperature, mass, etc., by measuring damping rate at different pressures.

2.2 Cooling the CoM motion of nanoparticles

The principle of trapping nanoparticles is based on a focused laser beam's radiation pressure. The laser beam's focus region creates a stable 3D parabolic potential well, where the trapped particle performs a resonant motion in an optical potential well. The damping rate of optically levitated nanoparticles are minimal in the vacuum environment, which can be used for ultra-precise measurement, and further cooling of the CoM of nanoparticles will improve the measurement sensitivity^[30, 31]. At the same time, it is also an effective way to prepare macroscopic quantum states^[32, 33]. Cooling the CoM motion of optically levitated nanoparticles to their quantum ground state can be used to study the quantum phenomena at the macroscopic level^[34, 35]. Nowadays, many international groups have proposed schemes for generating macroscopic quantum superposition using optically trapped nanoparticles, i.e. "Near-field interferometry of a free-falling nanoparticle from a point-like source" proposed by Bateman *et al.*^[36]. Oriol Romero-Isart *et al.*^[32] proposed a

method to cool the particles in the high-finesse cavity where the pressure on the particle will be very low to create the quantum superposition of macroscopic dielectric nanoparticles. Besides, research in quantum physics can also be used to measure short-range forces^[30, 31, 37, 38]. In 1976, A. Ashkin introduced the idea of feedback stabilization to cool the trapped particles^[9].

A feedback loop is essential when the pressure decreases and the heating effect of the nanoparticle are greater than the damping rate from the air; eventually, the particles gain sufficient energy to skid out of the optical trap. To avoid this heating effect, we may need to use some alternative method to cool the particle's centre of mass motion. Different techniques have been developed to cool or reduce the heating effect of the nanoparticles in traps. In principle, the cooling methods are of two types. One approach is to obtain the output signals from the particles and feed them back into the AOM, which adjust the power of the trapping laser beam. Another method is to implement the feedback loop before the chamber, which will reduce the pointing noise and amplitude of the trapping laser. And to do that, all you need to do is place a photodetector before the chamber with a lens having the same focal distance as the pointing position of the laser in the chamber. FPGA (field-programmable gate array) will also be connected and provide an input signal through the modulation of the AOM and piezo deflection mirror to the pointing position of the trapping laser for feedback cooling.

Some of the cooling techniques are given below.

2.2.1 Active feedback cooling

Cooling the centre of mass motion of an optically levitated microsphere was studied experimentally at the University of Texas at Austin by Dr Tongcang Li. They have cooled simultaneously the three degrees of CoM motion of the particle from room temperature to a minimum temperature of about 1.5 mK. Three laser beams of 532 nm have been used to cool each degree of freedom. The signal of the particle's motion is feedback to the acousto-optics-modulator (AOM) to control the power of the trapping beam at a pressure of about 5.2 mPa. The phonon number for the corresponding mode has been reduced to a number of 3400 from 6.8×10^8 . The rms amplitude has reached 15 pm from 6.7 nm^[39].

2.2.2 Parametric feedback cooling

In 2012, Jan Gieseler *et al.*^[40] of the ICFO-Institut de Ciencies Fotoniques, Mediterranean Technology Park in Spain proposed a scheme to cool the centre-of-mass motion of nanoparticles through parametric feedback cooling. It uses a single laser beam instead of additional lasers for cooling the three dimensions of nanoparticle efficiently. Parametric feedback uses the gradient force to cool all the motional degrees of freedom and works by changing the trap stiffness as a function of bead position. The trap stiffness (spring constant k) will change if the bead moves away from equilibrium position. The stiffness will increase when the bead moves away and will decrease if the bead moves towards the equilibrium position. Intensity gradient of dipole trap is proportional to the stiffness. The modulation of the trap laser power will modulate stiffness of the trap as well.

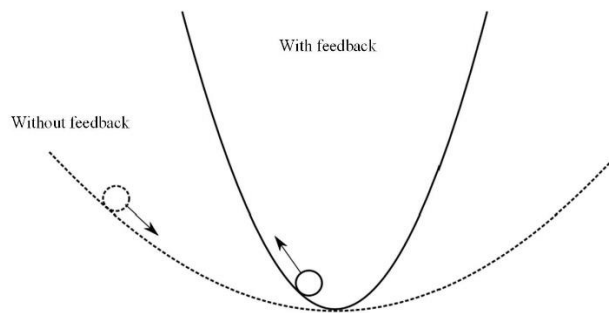


Figure 2.1. Simple illustration of this technique.

A single laser beam is intensely focused to trap and cool a single silica nanoparticle with a radius of about 70 nm. The motion signal of the oscillation frequency is doubled and phase-shifted. The resulting signal is feedback to the acousto-optic modulator (AOM) to modulate the power of the trapping laser (basic diagram given in Figure 2.1), which affects the optical potential. By stabilizing the depth of the trap, it enables cooling the particle centre-of-mass motion. They succeeded in decreasing particle temperature from room temperature to about 50 mK at a pressure 2.5×10^{-6} mBar. And they also made it confirm that the centre-of-mass motion temperature is proportional to the air pressure.

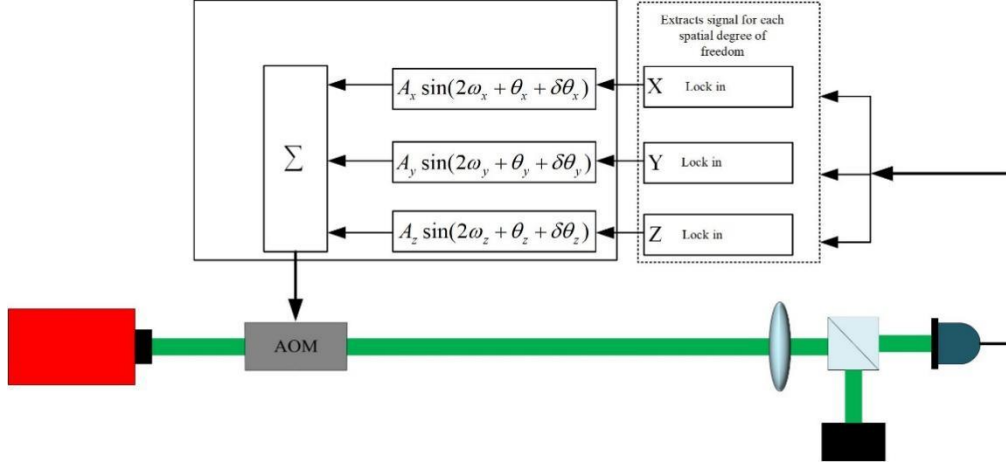


Figure 2.2. Basic diagram of parametric feedback cooling.

In 2017, Hendrik Ulbricht group at the “Department of Physics and Astronomy, University of Southampton, UK” used a parabola with high numerical aperture. A 102 nm silica nanoparticle was trapped by optical gradient force using a parabolic mirror. It cooled all the three motional degrees of freedom with the help of parametric feedback cooling to a few millikelvins ^[41]. At 6×10^{-6} mBar, the three degrees of freedom were cooled to 13mK, 6mK and 3mK, respectively. At this point, the quality factor of the optically levitated nanoparticle reached 10^9 .

2.2.3 Electric feedback cooling

In 2019, M. Iwasaki *et al.*^[42] of the Department of Physics, Tokyo Institute of Technology, Japan, proposed a new method to cool the centre-of-mass motion of charged nanoparticles. They added a pair of parallel electrodes near the focal point of the focused laser, where the particle is trapped. They measured the position of nanoparticles through an optical field and synchronized the oscillating electric field to the particle's motion. The effective temperature of the nanoparticle reached below 10 mK but a little higher than 6 mK at pressure 4×10^{-3} Pa for every direction. The phonon occupation number in the x , y , and z directions were 2.5×10^3 , 1.3×10^3 , and 6.1×10^2 , respectively. The cooling effect of electric feedback was about two orders better than parametric feedback cooling.

In the same year, Gerard P. Conangla and others at ICFO, Spain, used the identical method to cool one mode of the centre-of-mass motion of an optically levitated nanoparticle ^[43]. At a pressure of 3×10^{-7} mBar, the centre-of-mass motion temperature reached 5 mK. Lukas Novotny at Photonics Laboratory, ETH Zürich, Switzerland,

(coincidentally on the same date with Gerard P. Conangla), published the same method with an outstanding result. The centre-of-mass (CoM) motion of trapped nanoparticles was successfully cooled down from room temperature to a record low temperature of $100 \mu\text{K}$ at a pressure of 10^{-8} mBar^[44].

2.2.4 Cavity cooling

In 2019, Lukas Novotny's group and Markus Aspelmeyer's group independently cooled the three CoM motional degrees of levitated nanoparticles in an optical cavity through coherent scattering^[45, 46]. The particle's centre-of-mass motion cooled down to 10 mK at pressure 3×10^{-7} . Further cooling was limited by the laser phase noise^[47]. In 2020, Markus Aspelmeyer's group successfully cooled the nanoparticle from room temperature to its quantum ground state by precisely controlling the position and frequency of the trapping laser w.r.t optical cavity. The phonon numbers were reduced to 0.43, and the corresponding temperature was $12 \mu\text{K}$ ^[48].

2.3 Applications of optically trapped nanoparticles.

Optically levitated nanoparticles are considered as Nanomechanical harmonic oscillators and have numerous applications such as force sensors^[31, 49], gravity sensors^[50], precise motion sensors^[51], mass sensors^[52-54], charge sensors^[55], sound wave detection in liquid^[56] and temperature sensor^[30, 57], but Its sensitivity is mainly limited by environmental thermal noise^[58, 59]. Therefore, optically levitated nanoparticles are suitable measurement sensors at very low pressure under specific circumstances^[60, 61]. However, due to the decoupling characteristics of the optically levitated nanoparticle system and the environment, it can be achieved at room temperature. These articles give the sensitivity of mechanically immobilized harmonic oscillators in cryogenic environments with a straightforward, simple setup^[40, 62].

2.4 Summary

This chapter explains the Brownian motion of particles under the influence of optical force in a fluid and vacuum environment. Further, we describe the damping rate of CoM

motion of optically levitated nanoparticles. Different techniques have been developed and explained here to cool the centre-of-mass motion of optically levitated nanoparticles to millikelvin or micro-kelvin temperature and even cool it down to its quantum ground state for observing the quantum phenomena on a mesoscopic scale. Lastly, we explain some practical uses of optically levitated nanoparticles in different measuring and sensing systems.

Chapter 3: Experimental setup for optically levitated nanoparticles

3.1 Introduction

Optical trapping and manipulation of mesoscopic particles didn't even exist until the advent of lasers. It plays an essential role in studying micron-sized particles in chemistry, physics and biology. Arthur Ashkin showed in 1970 that a focused laser beam exerts radiation pressure on small particles and can affect the dynamic of particles^[6]. In 1976, He trapped a micron-size particle, and the pressure was reduced from room temperature to a high vacuum of 10^{-6} Torr^[8]. A simple method to trap particles with the help of focused lasers is based on vertical orientation. The upward scattering force balances the gravity of the particles and can be easily levitated by light. In 1986, Arthur Ashkin group proposed the use of a single-beam gradient force to trap microparticles, and they successfully captured the particles in an aqueous environment^[14]. In 1997, Ryota Omori's group at the University of Tokyo had used a single-beam gradient force which creates a potential well to trap micrometer size particles in the air^[63]. Trapping the particles in the air is more complicated than an aqueous environment. The coefficient of air viscosity is larger than water. The damping rate of moving particles in the air is also smaller. The movement of a particle in air is larger than in water, and the speed of particles in the air is also greater than in water. So, it will require a larger gradient force to overcome the particle's kinetic energy. Another reason is that the relative refractive index of particles and air is larger, and the scattering of laser light applies more force on the particles to kick them out of the potential well.

Furthermore, the gravity of the particle is also considerable, and the water can exert a larger buoyant force on particles than air. So, it is easier to trap particles in water than in air. In 2010, Dr Tongcang Li successfully trapped a micron-size particle in a vacuum using gradient force^[24]. In a vacuum environment, the particle's centre-of-mass motion has a minimal damping rate, which can be used for precise measurements and manipulations^[30, 31, 64, 65]. Hence, optically levitated nanoparticles in a vacuum became a popular research direction.

First of all, we describe the basic experimental setup for trapping the nanoparticles. We have illustrated the basic sketch of the optical path used in our experimental platform. Then, we design a vacuum system for trapping the nanoparticles and their components. We chose specific nanoparticles as our research objects and described the methods to make a solution and the loading methods in detail. After the nanoparticles are trapped in a vacuum chamber by the focused laser beam through a high NA objective lens, the centre-of-mass motion signal of the three orthogonal eigenmotion directions of the nanoparticle, its measurement method and principle are introduced in detail. The core of the measurement system is a self-made balanced homodyne detector with high gain, high bandwidth and high common-mode rejection ratio. It can achieve high precision measurement of the particle's motion signal.

3.2 Optical path and essential components

A simplified diagram of our experimental setup is given in Fig 3.1. In most of our experiments, we used a dual-wavelength (1064 nm and 532 nm, 20W, CW, DPSS FG-VIB) laser system assembled by our institute (Institute of Optoelectronics, Shanxi University). The 1064 nm and 532 nm output laser beams are protected from reflecting back into the laser through an isolator. The output 1064 nm laser beam from the laser is divided into two parts through PBS (polarizing beam splitter), where one part of the beam enters the F-P cavity to check the stability of the laser. The other part is divided into two parts through PBS, then coupled to a single-mode fiber optic. One part of the 1064 nm beam passes through an AOM (Acousto-optic modulator) to shift the frequency of the beam by a mount of 110 MHz. In contrast, the other part is un-shifted. The shifted and un-shifted laser beams are combined with PBS and then pass through the quarter and half-wave plates. The polarization of the trapping beams can be adjusted according to the experimental requirements. An objective lens (Nikon CF IC EPI Plan 100X, NA=0.95 and the working distance (WD)=0.3 mm) tightly focuses the vertically propagating laser beams in the gravity direction. Another high NA aspheric lens (Thorlabs C330TMD-C, NA=0.68, WD=1.8 mm) is used to collect the trapping beam's output light to detect the CoM motion signal, torsional signal and rotation signal of the nanoparticle. One beam of

the two entering beams to the chamber is precisely controlled by Pico-motor (New focus) to move the beam to any desired location within the specified region.

The second wavelength, 532 nm from the laser is used to illuminate the nanoparticle. The same high NA objective lens collects the scattered light from the nanoparticle and imaged it on a CCD camera (squeezed light field). Different components of our experimental setup are explained in the upcoming sections in detail.

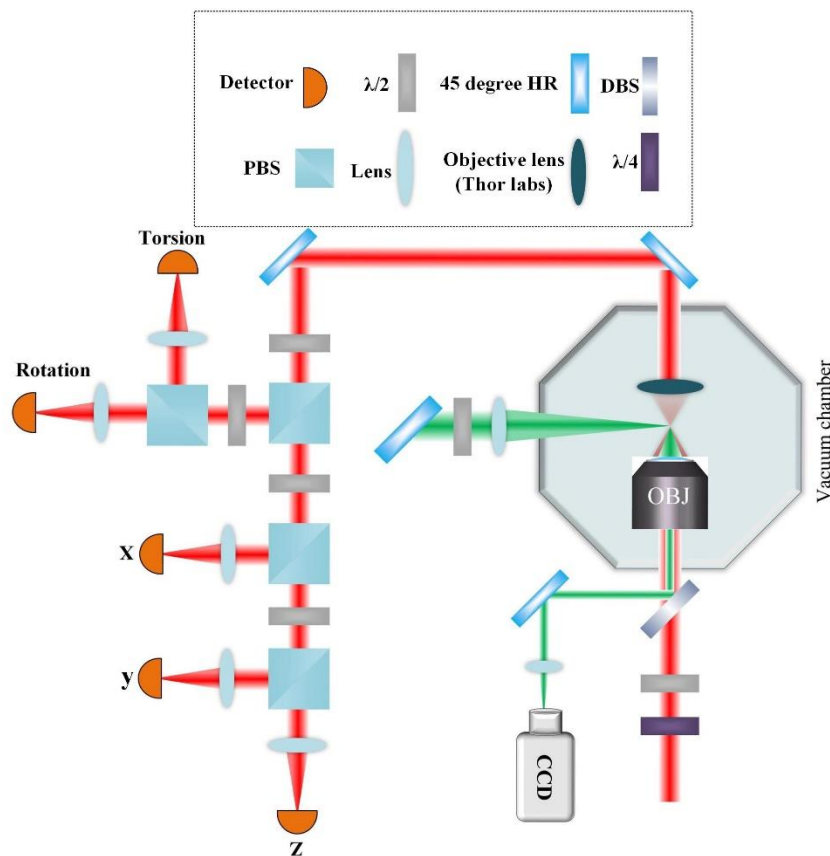


Figure 3.1. The basic diagram of our experimental platform, and different components.

3.3 Vacuum system

Generally, the vacuum is a region in space where the pressure of gas is lower than atmospheric pressure. The perfectness of a vacuum can be measured through the pressure inside a chamber. If the pressure reaches a low value, then the vacuum is better and vice versa. The vacuum system has many advantages like low viscosity coefficient, weak thermal motion, less collision of air molecules, etc. Vacuum systems are widely used in

physics, food processing industries, materials, and various research fields have the advantages of this system, such as life sciences and precision instruments.

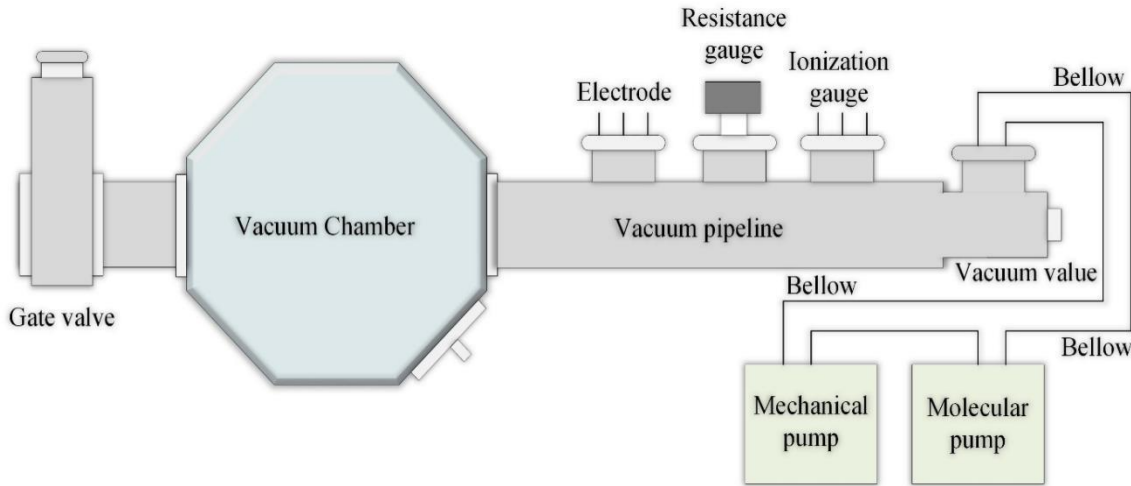


Figure 3.2. Basic representation of vacuum system.

Figure 3.2 shows the schematic diagram of vacuum system used in our experimental platform. The vacuum system mainly includes a vacuum chamber or science chamber, vacuum valve, vacuum chamber windows, vacuum pipelines, vacuum gauges and vacuum pumps. The vacuum chamber used in our platform is an octagonal ultra-high vacuum chamber (6 Multi-CF Spherical Octagon: MCF600-SphOctF2C8) developed by Kimball Physics (company). The chamber contains eight windows around it to facilitate the connection of other vacuum components and observation of experimental operations. Inside the chamber is an ample cylindrical space, which can be used to place optical components required for the desired experiments. One of the windows from the vacuum chamber has been used to connect a high voltage single polarity wire to charge and discharge particles. Two of the windows connect other components of the vacuum, while five of the eight windows have vacuum window lenses (MDC Zero Profile Viewport). The vacuum window lenses are coated with 532nm and 1064nm dual-wavelength zero-degree anti-reflection coating and can reduce laser power loss while performing the experiments.

One of the vacuum chamber window is used to connect the gate valve. This gate valve is for loading the nanoparticles into the vacuum chamber through different approaches. On the opposite side, the vacuum chamber has a series of vacuum connection

Rotation and scattered light interference of optically levitated nanoparticles

pipes listed as follows respectively: vacuum electrodes, resistance vacuum gauge, ionization vacuum gauge, and vacuum valve.

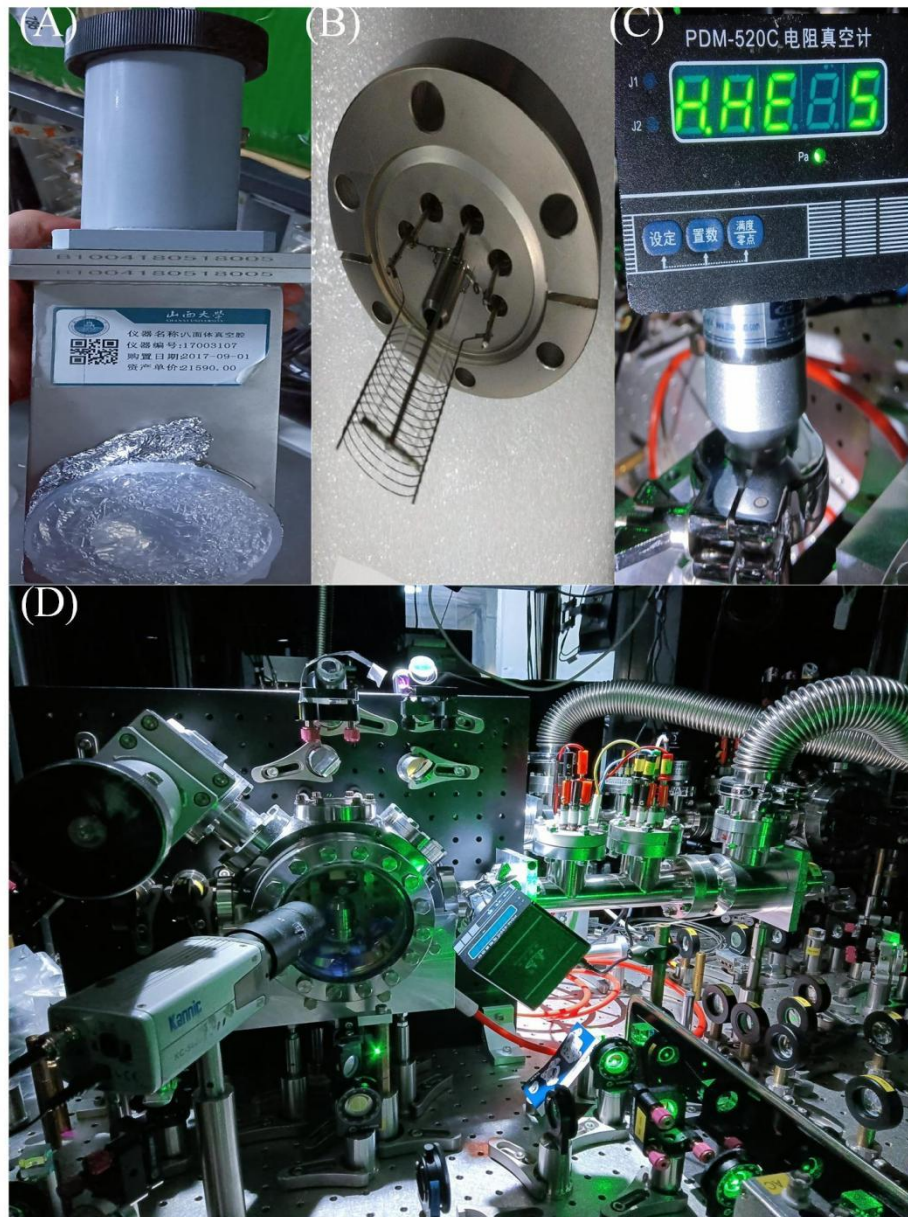


Figure 3.3. Real picture of the vacuum system components. (A) is the Gate valve, (B) Ionization gauge, (C) Resistance gauge and (D) is the complete picture of all the components together, including the vacuum chamber.

The vacuum electrode consists of six terminals that conduct external electrical signals into the vacuum chamber and provide the electric field for different related research experiments. The resistance gauge measurement range is $10^5 - 5 \times 10^{-2}$ Pa, and the ionization gauge range is about $10^{-1} - 10^{-8}$ Pa. These gauges can measure the pressure from atmospheric pressure to high vacuum. Here, it should be noted that the ionization vacuum

gauge generates Corona discharge and impacts the experimental results. In order to keep the impact very low, we place the ionization gauge at a specific distance from vacuum chamber. The vacuum valve is connected to the vacuum pump through a bellow, which can control the pumping of air velocity and air pressure in the vacuum system. In our system, we have used two vacuum pumps. One is a mechanical pump that can easily reduce the pressure up to 0 Pa, but to reduce it further, we need a molecular pump, which reduces the pressure in the entire vacuum system to 10^{-3} Pa. The vacuum system (except the vacuum pump) is placed on an air suspension optical table (Newport). It can effectively isolate external vibration and improve system stability.

3.4 Selection of particles and loading

Nanoparticles have numerous types, but mainly they can be divided into two groups, i.e. organic and inorganic nanoparticles. Here, we are more interested in inorganic nanoparticles, including quantum dots, fullerenes, silica, gold etc. The Refractive index and size of the particles have different effects on the light trapping system. The particles considered as mechanical objects used in levitation are typically nano-or microparticles with a specifically chosen geometry. Ideally, a spherical particle can be used to measure the centre-of-mass motion. And to measure the liberation or rotation, a cylindrical or ellipsoidal particle is better to choose. The particle selected in our experiments is silica nanoparticles (SiO_2 or Silicon dioxide). The reason for selecting the silica nanoparticle is its high refractive index and monodisperse. These particles are produced by Bangs Laboratories, Inc. USA ([Bangs Laboratories, Inc.](#)). By observing silica nanoparticles under the scanning electron microscope, the silica particles are spherical, and the size distribution is uniform. In our experiments, we have tried different particles, but the most common one has 163nm diameter. Stock solution picture of silica nanoparticle and dilute solution is given in Fig 3.4.



Figure 3.4. Stock solution of silica nanoparticle and sonicated dilute solution.

For non-spherical nanoparticles, such as little asymmetric particles or Nano dumbbells or rods, in addition to the translational motion of three degrees of freedom, the particle's motion in the optical potential well also produces torsion and rotation^[66-70]. Furthermore, spherical nanoparticles are easier to trap under a high vacuum, while non-spherical particles will follow the air flow as we decrease the pressure and can be lost easily.

The stock solution of monodisperse nano-silica particles purchased is in an aqueous solution. The surface functional group is hydroxyl (-OH). The concentration of particles in solution is 2.5% w/v (weight per volume), which means that in 100ml, there are 2.5g of nano-silica particles. When the particles are stored for a long time, it breeds bacteria inside and leads to deterioration, affecting the trapping and experimental measurement. To avoid this phenomenon, we dilute the aqueous solution of nanoparticles in high-purity ethanol with extreme care by not introducing impurities when diluting. The ethanol we have used are of chromatographic grade with a purity of 99.9%. After making the solution, we store it in the refrigerator and maintain a temperature of about 4 degrees Celsius, which last for a very long time.

3.4.1 Making solution

After choosing the nanoparticles, the next step is to make the dilute solution with the desired concentration. In our experiments, mainly we have used silica nanoparticles. When diluting the solution, first, we need to wear gloves to avoid adding impurities into the solution. The initial high concentration solution should be shaken well and placed in an

ultrasonic cleaner for sonication so that the silica particles are uniformly and monodispersed in the solution. A micro-volume of the stock solution is then diluted into high-purity anhydrous ethanol by pipette. The silica nanoparticles are commercially hydro-soluble. We use a concentration of $2.4 \times 10^7/ml$. It means that $1ml$ of ethanol contains 2.4×10^7 nanoparticles. And then sonicate the dilute solution again for at least 30 minutes to distribute the particles evenly. The ethanol solution of the particles become atomized, and the resulting droplets contain individual nano-silica particles. The whole process of configuring the nano-silica particle ethanol solution needs to be carried out in an ultra-clean room to ensure no pollution.

3.4.2 Loading of nanoparticles

Once all the experimental setups (Vacuum system, laser system, optical trap etc.) are ready, the next step is to load the nanoparticles into the vacuum system and trap it. The ultrasonic nebulizer used in the experiment is the Omron mesh nebulizer NE-U22, as shown in Fig 3.5.



Figure 3.5. Omron mesh nebulizer NE-U22

To trap an individual nano-silica particle, the solution is injected into the nebulizer bottle to atomize the ethanol solution. It is appropriate to keep the ratio of droplets to nano-silica particles at 100:1. We use a Teflon thin tube of about $5mm$ diameter to carry the vaporized solution containing the nanoparticles from the nebulizer into the vacuum chamber near the focal point of the objective lens. The concentration of the ethanol solution spray needs to be controlled so that the droplets entering the vacuum chamber have a certain initial velocity, which is convenient to trap a single nanoparticle. After trapping nanoparticles, we close the gate valve and turn on the vacuum pump to evacuate the chamber. Lastly, we open the vacuum valve and precisely control the evacuation of the chamber to prevent the nanoparticles from losing.

The following points should be noted when using the nebulizer: The solution should not be stored in the nebulizer for a long time. If the solution is changed once a day, the atomizer needs to be cleaned at regular intervals to prevent the precipitation and aggregation of silica particles. The nebulizer and the bottle in which the solution is kept should be cleaned with an ultrasonic cleaner.

3.5 Detection system

The easiest and quickest method to observe if the particle has been loaded into the optical trap is using a CCD (Kannic KC-582B), placed perpendicular in the front window of the vacuum chamber. When the nanoparticle gets trapped, it absorbs and re-emits the light irregularly, which is sufficient for an ordinary CCD camera to capture it in a long exposure. The CCD is connected to a VCR monitor screen, and a real-time video can be seen simultaneously. We can see a “white small dot” above the high NA objective lens, which gives us the first insight into a trapped nanoparticle.

When considered in Cartesian coordinates, nanoparticles captured by an intensely focused laser perform resonant motion in an optical potential well and have three degrees of freedom. The corresponding eigenmotion frequencies are ω_x , ω_y and ω_z . In a vacuum environment, the collision of thermal motion of gas molecules causes the particles to make a damp resonant motion, which has high speed and regularity. Besides this, the motion range of the trapped nanoparticles is petite, and the maximum displacement is in the order of hundreds of nanometers. That’s why measuring the CoM motion of the nanoparticles requires a high-bandwidth, high-resolution and high-gain detection system. In our experimental platform, we utilize the balanced homodyne detection system to measure the CoM motion signal of the nanoparticles.

We use a strongly focused 1064nm laser beam to trap the nanoparticles. The scattered light from the nanoparticles and un-scattered light from the trapping beam is collimated by another high numerical aperture lens to make the output light from the particle parallel. The motion amplitude and diameter of the nanoparticles are much smaller than the waist spot of the focused laser beam and wavelength. The silica nanoparticle radiates light to the surrounding three-dimensional space, which contains the particle’s CoM motion

information. The output lens collects all the possible scattered light from the particle. The distance from the lens to the particle is exactly the lens's focal length. However, the particle's scattered light is weak and cannot be used directly to measure the quantitative CoM signal. As we know, the size of the particle is smaller than the waist spot of the focused laser, so most of the beam passes un-scattered. The scattered light from the particle and un-scattered light is being collected by a high NA aspheric lens, which is also parallel. The scattered and un-scattered light has the same frequency and good spatial coincidence. Both the output light interferes and the un-scattered light enhance the scattered light amplitude, which contains the particle's motion information and can be used to measure the CoM motion of the nanoparticle. The output beam can be split into the beam cross-section and along the beam propagation direction, discussed below in detail.

3.5.1 Radial detection

The particle has two orthogonal eigenmotions in the radial direction; let's suppose that one motion is in the horizontal direction represented by x and the other is in the vertical direction represented by y . In these two directions, the measurement method for motion signal is the same. We will consider the measurement of the CoM motion signal of the particle in the y direction as an example to analyze the detection method. Figure 3.6 represents the schematic diagram of homodyne detection of the y -direction eigenmotion of particles. The output scattered light from the particle, and un-scattered light carries information about the CoM motion of the particle.

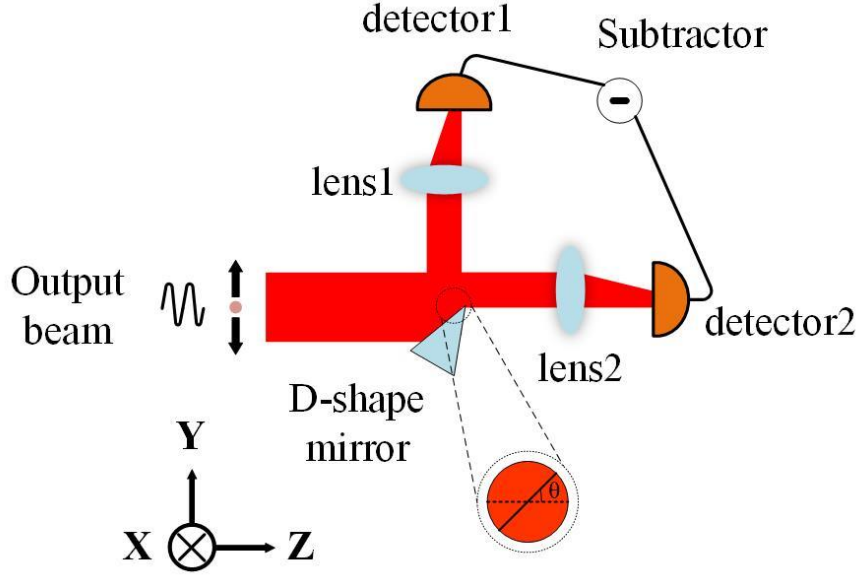


Figure 3.6. Schematic diagram of measuring the particle's radial motion signal.

We utilize a D-shape mirror with sharp edges (BBD1-E03 - Ø1" Broadband Dielectric D-Shaped Mirror, 750 - 1100 nm), which divides the cross-section of the beam into two equal parts. An individual spherical converging lens focuses each part into two photodiodes for measurement. The focal length of the converging lens is $f=30\text{mm}$, and the waist of the focused beam is about $\omega_0 = 30\mu\text{m}$. The photodiode used in our experiment is the Indium Gallium Arsenide photodiode ETX500 made by the JDSU company, which has an effective diameter of $500\mu\text{m}$ on the photosensitive surface. The sensitivity range of the detector to the wavelength ranges from 800-1700nm, which has high quantum efficiency and small dark current and can meet the high-precision measurement of particle motion signals. The difference signal of the amplitudes of the two halves of beams can be obtained by subtracting the signals detected by the two photodiodes through a subtractor. Inside the dashed circle in Figure 3.6 is the beam's cross-section at the D-shaped mirror; the dashed line represents the horizontal x -direction. The solid line is in the vertical direction representing the y -direction. The D-shape mirror divides the beam into two halves. The angle between the sharp edge of the D-shape mirror and the x -direction is θ . The un-scattered light is ultimately cancelled in measurement and leaves only the part related to the motion signal of the particle. The difference signal can be written as:

$$D(t) = D_x(t)\sin\theta + D_y(t)\cos\theta \quad (3.1)$$

$D_x(t)$ and $D_y(t)$ are the motion signals of the particle in x and y directions, respectively. When $\theta=0$, the D-shape mirror will be vertical, and only the y -direction motion signal of the particle will be divided into two halves. And if $\theta=\pi/2$, the D-shape mirror will divide the horizontal part of the beam into two halves, which contains information about the x -direction of the particle's motion. In this way, we can precisely determine the radial motion of the particle.

3.5.2 Axial detection

The detection method of the particle's axial CoM motion signal is quite different from that in the radial direction. In this case, a half-wave plate and a polarizing beam splitter are used to split the outgoing light into two halves. The transmitted part through the PBS is focused by a spherical converging lens of 30mm focal length into the photosensitive area of the photodetector. The waist of the focus beam is smaller than the photosensitive area of the detector. The basic schematic diagram is given in Figure 3.7 below.

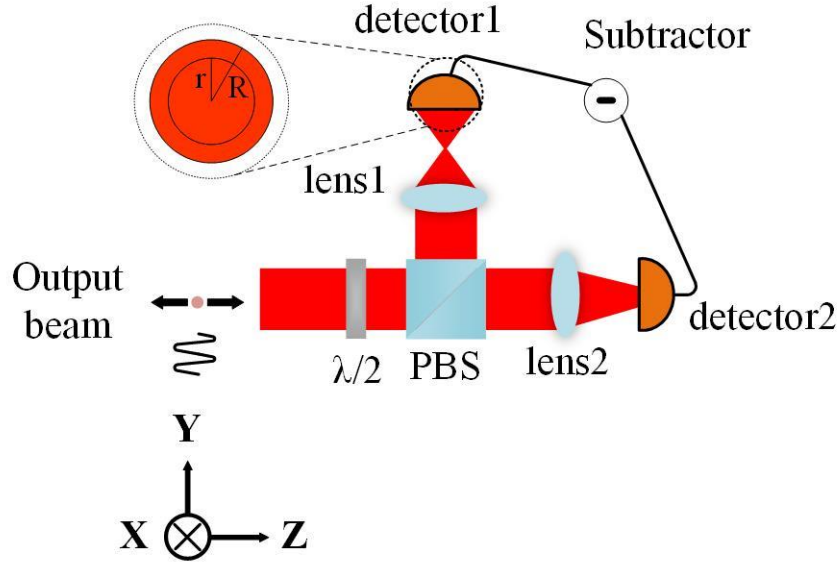


Figure 3.7. Schematic diagram of measuring the particle's axial motion signal.

The reflected light is focused and expanded by a spherical mirror with a short focal length making the beam cross-section larger than the photosensitive area of the photodiode shown in the dotted area of the circle in Figure 3.7. In the given diagram circled area, r is the radius of the photodiode sensitive area, R is the radius of the beam cross-section where

$r < R$. The first photodiode only measures the intensity of the central portion of the reflected beam. When the particle gets trapped, the particle's movement in the axial direction changes the convergence of the outgoing light. So, the intensity of the reflected light measured by the first photodiode is related to the axial displacement of the particle. We must choose the proper ratio of r to R , and the subtractor cancels out all the unscattered parts of the signal, leaving the part related to the particle axial motion signal. In our case, the relative intensity of transmitted light and reflected light is 1:2, and the axial motion of the particle has a larger signal-to-noise ratio.

3.5.3 Balanced homodyne detector

The balanced homodyne detector is used to measure the CoM motion signal of particles. The main components of the homodyne detector are two photodiodes and subtractors, which measure the particle motion signal and process it in one circuit. Figure 3.8 is our homodyne detector's schematic PCB (printed circuit board) diagram. The two photodiodes are directly connected in series, and their current can be obtained at the node. An operational amplifier then processes the difference signal. This design avoids the inconsistency of the detector components and extra noise introduced in signal processing. It has a sizeable common-mode rejection ratio. The voltage can be divided into two parts, one part obtains the AC signal through a high-pass filter composed of C2 and R3, and the cutoff frequency is:

$$f = \frac{1}{2\pi R_3 C_2} \quad (3.2)$$

The other part is used for the detection of DC signals. This detector can be called a current subtraction detector.

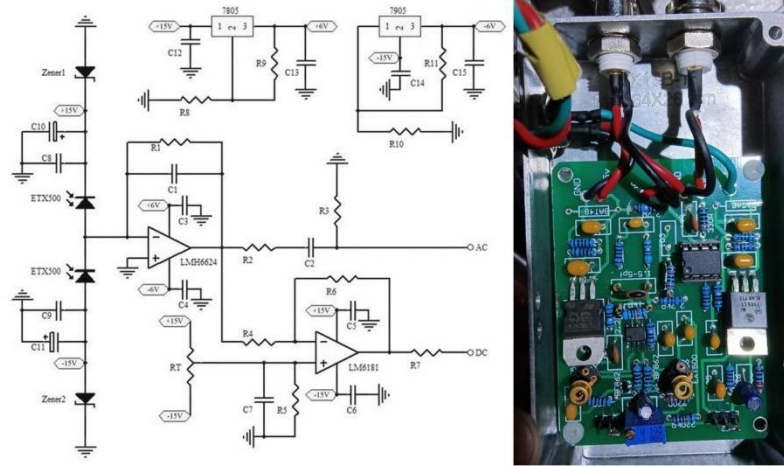


Figure 3.8. Shows the electronic circuit and PCB with all the components.

The photodiode uses InGaAs PIN photodetector ETX500 made by the JDSU company. The detector has high quantum efficiency and sensitivity in the range of 800-1700nm spectral region. In normal operating mode, its dark current is 1.7nA, the junction capacitance is 44pF, and the bandwidth is 140MHz. the noise current density is about $10fA/\sqrt{Hz}$. Which meets the high-precision measurement of the centre of mass motion of the nanoparticles. The detector adopts two-stage amplification to obtain signals with larger gain and larger bandwidth. The first stage method uses jumper resistance, the operational amplifier model (LMH6624) has been used, and the unit gain bandwidth is 1.3GHz. The gain of the first-stage amplifier circuit is $(-1 \times 10^4 V/A)$. The output signal of the first-stage amplifier circuit is divided into two parts, which are used to detect DC signal and AC signal. In our experiments, to measure nanoparticles' low-frequency CoM motion signal, the DC output signal needs to be analyzed. That's why only the DC signal is amplified in two stages. The second-stage amplifying circuit of the DC signal adopts a general subtractor circuit design. When there is no optical input signal, the DC output signal will have a particular bias voltage due to the unbalanced voltage and load of an operational amplifier. To not affect the measurement of particle motion signal, a reverse input voltage is added in the second-stage amplifier circuit. The DC output signal is zero when there is no optical input signal. The second-stage amplifier model is (LM6181), the unit gain bandwidth is 100MHz, and the amplification factor is $-R_6/R_4 = -5$. And the total amplification of the detector is:

$$TF = \frac{R_6}{R_4} \times (I_1 - I_2)R_1 \quad (3.3)$$

Where I_1 and I_2 are the currents generated by two photodiodes. The gain of the detector is $5 \times 10^4 V/A$, and the bandwidth is approximately 20MHz.

3.6 Data recording and analysis

The nanoparticle's CoM motion can be measured in three 3-D with three different homodyne detectors, as explained in section 3.5. Each detector can be used to measure the optical signal in separate directions. The PSD (power spectral density) signal of nanoparticle's CoM motion from detectors is recorded with "The Rohde & Schwarz signal and spectrum analyzer" model ([FSV3013](#)). This machine is advanced, enabling us to save data on a flash drive. Usually, in one file, we can save up to six traces. The frequency range of this machine is from 10Hz-13.6Ghz and gives us a flexible environment to record an enormous range of data. The spectrum analyzer connects the homodyne detector through a BNC cable. We record the traces for each position (direction) of the nanoparticle at a different pressure. To record the centre-of-mass motion of the nanoparticles, we set the initial frequency of the spectrum analyzer at 0Hz and the final frequency at approximately 300-400 kHz, depending on the particle trajectories in the trapped beam. We take the average of the PSD through an analyzer and save the traces of averaged trajectories. As all the necessary data recording finishes, we transfer the data to another PC (personal computer) for analysis.

3.6.1 Data analysis

We record and analyze the motion of nanoparticles in the frequency domain. The analysis of equation (2.9) holds for all three dimensions. The power spectral density signal gives us information about the signal's average power distribution at a specific time in the frequency domain. Integrating the power spectrum density overall frequencies range will provide us with the average power of an entire signal. For example, we will consider the power spectrum density of a nanoparticle motion in only one direction, i.e., x -direction. The power spectral density of particle motion under different pressures is measured in Figure 3.9. given below.

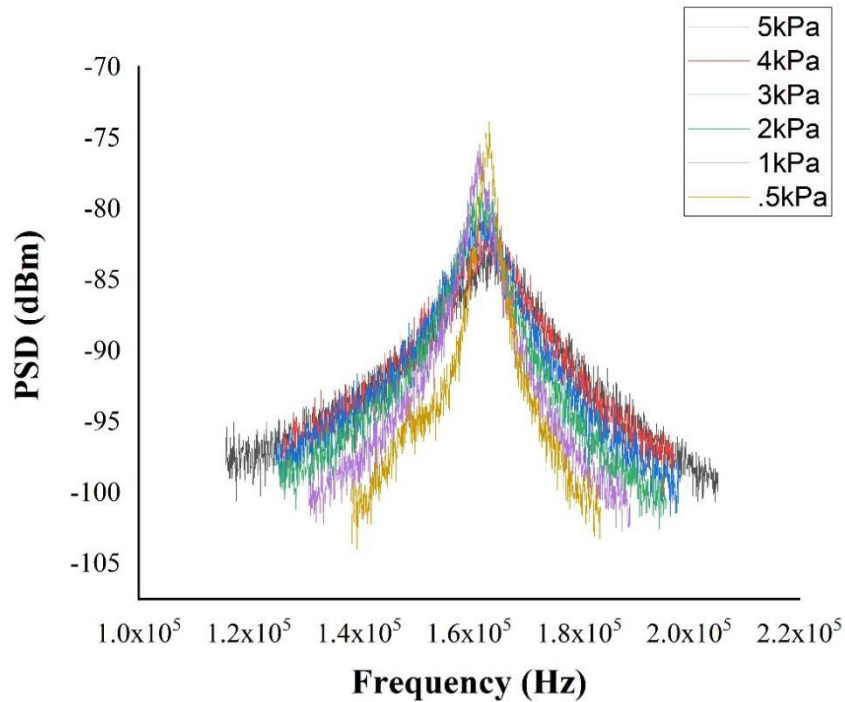


Figure 3.9. PSD of a nanoparticle's motion in the x -direction.

The Power spectrum density has been recorded for every pressure started from 5000Pa in descending order up to 500Pa. We have used the origin software to analyse the power spectrum density. We use a nonlinear fit for each pressure's power spectrum density to get the damping rate of the nanoparticle at that specific pressure. By doing so, we complete the fitting of all the pressure and get the damping rate of each pressure. The next step is to plot the damping rate again to pressure. The damping rate for Figure 3.9 is given in Figure 3.10. Once we get the damping rate, we use linear fitting to analyse the data further. The slope of the linear fit can help us calculate the radius of the particle and the mass of the particle.

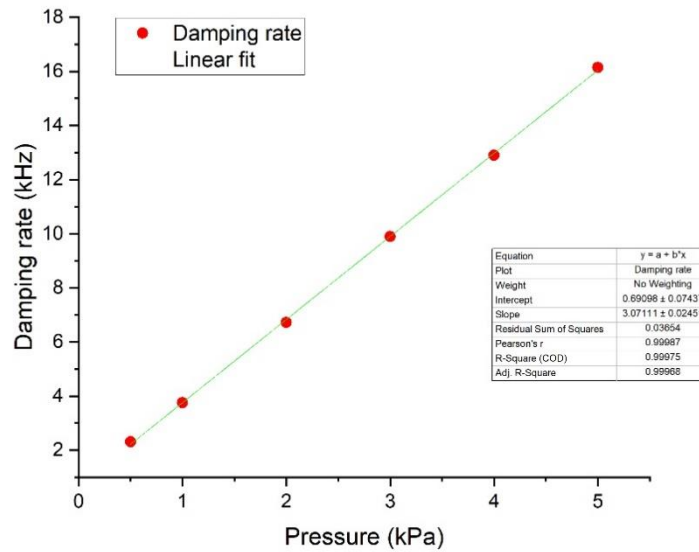


Figure 3.10. Damping rate of nanoparticle's x -direction.

By fitting the damping linearly, we obtain the slope of the graph, which can be used in finding out the size of the nanoparticle, i.e., the radius of the particle or length of the x -direction (for this example length of the x -direction is 186 nm), if the particle is not a complete sphere. Once we have the particle's radius, further on, we can find out the mass of the particle as well. The density of particles is mostly given, and by obtaining the lengths of all three directions, we can easily get the mass of the particles.

3.7 Summary

In this chapter, we briefly introduced optical trap uses and development in different fields of today's science. A simplified diagram of our experimental setup is given in Fig 3.1. We have used a dual-wavelength (1064 nm and 532 nm) laser. The output 1064 nm laser beam from the laser is divided into two parts through PBS; one part is for the F-P cavity and the second for experiments. An objective lens (Nikon CF IC EPI Plan 100X, NA=0.95 and the working distance (WD)=0.3 mm) tightly focuses the vertically propagating trapping beams in the gravity direction. Another high NA aspheric lens (Thorlabs C330TMD-C, NA=0.68, WD=1.8 mm) collects the trapping beam's output light to detect the CoM motion signal, torsional signal and rotation signal of the nanoparticle. One beam is precisely controlled by Pico-motor (New focus) to move the beam to any

desired location within the objective plan. The second wavelength, 532 nm from the laser is used to illuminate the nanoparticle. The same high NA objective collects the scattered light from the nanoparticle and imaged it on a CCD camera.

We designed a complete vacuum system including a vacuum chamber, vacuum valves, vacuum pipes, vacuum electrodes, vacuum gauges and vacuum pumps. The designated vacuum system is used to study optically levitated nanoparticles in a vacuum environment. Two vacuum gauges have been used to measure pressure in the vacuum chamber on particles from atmospheric pressure to very low air pressure, i.e., a resistance gauge and an ionization gauge. The vacuum gate valve has a large opening hole, which facilitates nanoparticle loading into the chamber and capture by the trapping beam. We select spherical nano-silica particles as the research object for our experimental platform based on particle size, refractive index, and stability under a high vacuum. A high concentration stock solution of silica nanoparticles has been bought from Bangs lab. A micro-volume of the stock solution is then diluted into high-purity anhydrous ethanol by pipette. The silica nanoparticles are commercially hydro-soluble. The concentration used in most of our experiments is 2.4×10^7 /ml. We use a Teflon thin tube of about 5mm diameter to carry the vaporized solution containing the nanoparticles from the nebulizer into the vacuum chamber near the focal point of the objective lens.

We measure the particle's CoM motion signal through the homodyne detection system as the nanoparticle traps. The balanced homodyne detection method is used to measure the motion signal, and the measurement principle of the signals of different eigenmotion directions of particles is analyzed in detail. In the radial direction, a D-shaped mirror is used to divide the cross-section of the outgoing beam into two equal parts. A detector is used to measure the difference signal of the two parts of the beam to obtain the radial eigenmotion signal of the particle. By rotating the D-shaped mirror's angle, the motion signals of the particles in the x and y directions can be measured, respectively. In the axial direction, the beam is divided into two parts; one part enters the photodiode entirely while the other part enters partially into another photodiode of the same detector. Both detectors have a subtractor that subtracts the input optical power from each other and cancels out the part of the beam that doesn't contain information about the particles'

Rotation and scattered light interference of optically levitated nanoparticles

motion. An overview of data recording and analysis is explained with an example of x -direction analysis.

Chapter 4: Rotational Optomechanics

4.1 Introduction

Controlling the rotational motion of a levitated particle has always been an attractive platform for researchers since Arthur Ashkin's pioneering work^[9]. A circularly polarized laser beam carries angular momentum, which causes an asymmetric particle to rotate continuously in an optical tweezer until the laser is turned off^[71-73]. Nanoparticles generally have a low damping rate, which enables them to rotate at a very high speed exceeding MHz, now even can measure more than 6GHz^[69, 70, 74]. The tensile strength of the particle limits these high frequencies rotation^[75]. Optically levitated rotors are used in a wide range of diverse areas, such as microrheology, nanotechnology, biophysics, microfluidics, and chiral resolution. As the cooling techniques developed, optically levitated nano-rotors became an important tool for precise measurement and manipulation of mesoscopic particles. In most previous work, feedback cooling techniques are utilized to stabilize the CoM motion of particles.

4.2 Optically levitated nanoparticles motion

In an optically levitated nanoparticle's system, the particle absorbs incoming photons from a circularly polarized laser beam. A circularly polarized beam contains angular momentum, which has an impact on a little asymmetric particle. The particle starts rotational movement as it absorbs photons from the circularly polarized trapping beam. In this case, the total torque received by the particle which drives the particle is denoted by M_0 . The particle is not entirely isolated from air molecules in a vacuum chamber and has little interaction with particles. This interaction damps the rotational motion of the particle, and a drag torque arises, denoted by M_d . The rotational motion equation of particles due to the combined effect of driving and drag torques can be written as^[74]:

$$2\pi I \frac{df_r}{dt} = M_0 + M_d \quad (4.1)$$

where $I \propto mR^2$ and denote nanoparticle's moment of inertia, m is particle's mass, R is the radius. In a particular air pressure, the drag torque M_d is proportional to the rotational frequency of the nanoparticle and can be written as^[76]:

$$M_d = -2\pi I f_r \gamma_d \quad (4.2)$$

where, $\gamma_d = pR^2/\eta m v$ gives us the rotational motion damping rate, η is the transmission efficiency of the angular momentum of the collision between air molecules and particles, v is the average speed of air molecules. Equation (4.2) shows that in the start, both the driving and drag torques depend upon each other; if driving torque increases similarly, the drag torques also increases. At a specific point, the torques balance each other, and the rotation frequency becomes constant. The rotation frequency of steady-state can be defined by:

$$f_r = \frac{1}{2\pi\gamma_d} \frac{M_0}{I} \quad (4.3)$$

Where f_r represents the rotation frequency of the particle, in our experiments, the polarization of the trapping beam is circular, the total torque which drives the particle is proportional to trapping beam intensity. $M_0 \propto I_0$ which indicates that rotation depends upon trapping the beam linearly. When the trapping laser power increases, consequently, the rotational frequency of the nanoparticle also increases.

Furthermore, the chirality of the trapping beam plays a vital role in the particle's motion. Considering elliptical polarization of the trapping beam can be resolved into two components, circular and linear polarization. The asymmetric shape and birefringence of the particle align it with linear polarization, and the particles start torsional motion. Similarly, circular polarization is responsible for rotation. We can control the polarization of the trapping precisely using half and quarter-wave plates.

4.3 Experimental observation of nanoparticle's rotation

4.3.1 Experimental setup

A schematic diagram of an optically levitated nano-rotor and CoM motion detection system is depicted in Figure 4.1. We use a 1064 nm laser beam focused by a high NA objective lens in the gravity direction to trap an individual silica nanoparticle. The loading

process of silica nanoparticles is already explained in section (3.4.2). The 1064 nm trapping laser beam passes through AOM (acousto-optic modulator) to control the beam power and shift the frequency by a amount of 110 MHz. Before entering the vacuum chamber, the beam passes through a quarter and half-wave plate, respectively, to adjust the polarization. We use a high numerical aperture objective lens (NA=0.95) to focus the laser beam and trap a particle firmly. The power of the trapping laser beam is 300 mW before entering the chamber, while the effective power on the particle's position is about 156 mW. The loss of power is about 52% due to window and objective. The trapping beam diameter is about 3.2 mm, while at the focus point, it is about 1.1 μm .

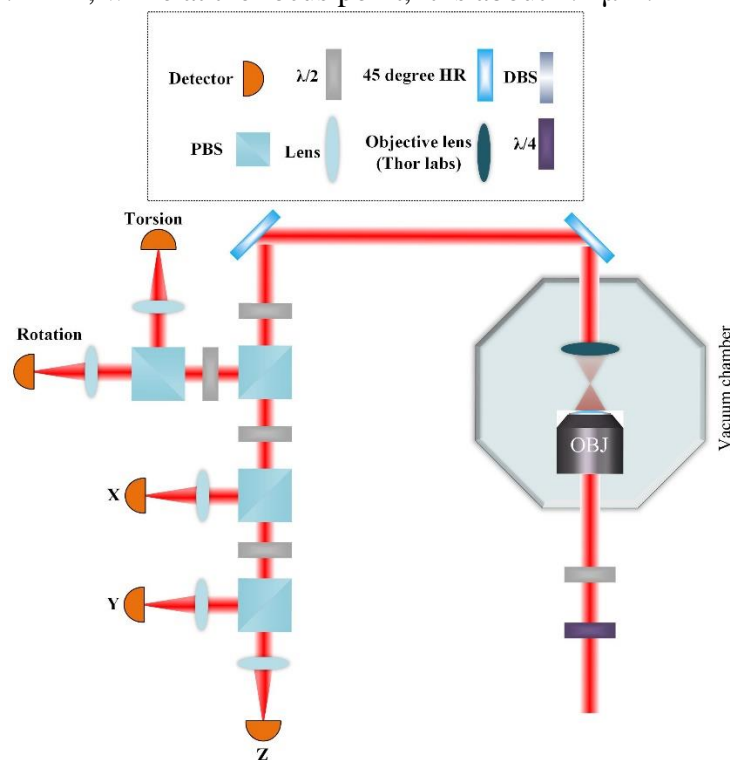


Figure 4.1: Schematic diagram of the optically levitated rotor and motion detection

Another high-NA lens collimates the output light of the trapping beam (Thorlabs, C330TMD-C, NA = 0.68, WD = 1.8 mm), and that light is used to measure the motion of the particle. The torsional motion signal is measured with (Hamamatsu C12702-03), the gain of this detector is about 10^4 V/A with a bandwidth of DC-100MHz. Rotation is measured with a high-speed fiber detector (New Focus 1554-A), which has a flat gain 10^3 V/A with a bandwidth of DC-12 GHz. The CoM motion is measured with the help of a balanced homodyne detection system. The beat signal detected from the nanoparticle is twice the actual motion signal. The reason is that nanoparticle acts like a polarization

modulator, and one rotation (2π) generates a (4π) modulation in trapping laser polarization. f_r (rotation frequency) after modulation will become $2f_r$.

4.3.2 CoM motion and torsional vibration measurement

Translational motion is always associated with trapped nanoparticles in a potential well, i.e., CoM motion. Due to the vector diffraction of light, CoM motion contains three eigenfrequencies in three different directions. In this experiment, the eigenfrequencies measured in x, y and z directions due to linearly polarized trapping beam are $f_x = 163$ kHz, $f_y = 205$ kHz and $f_z = 74$ kHz, respectively. The given PSD of CoM motion is measured at 500 Pa.

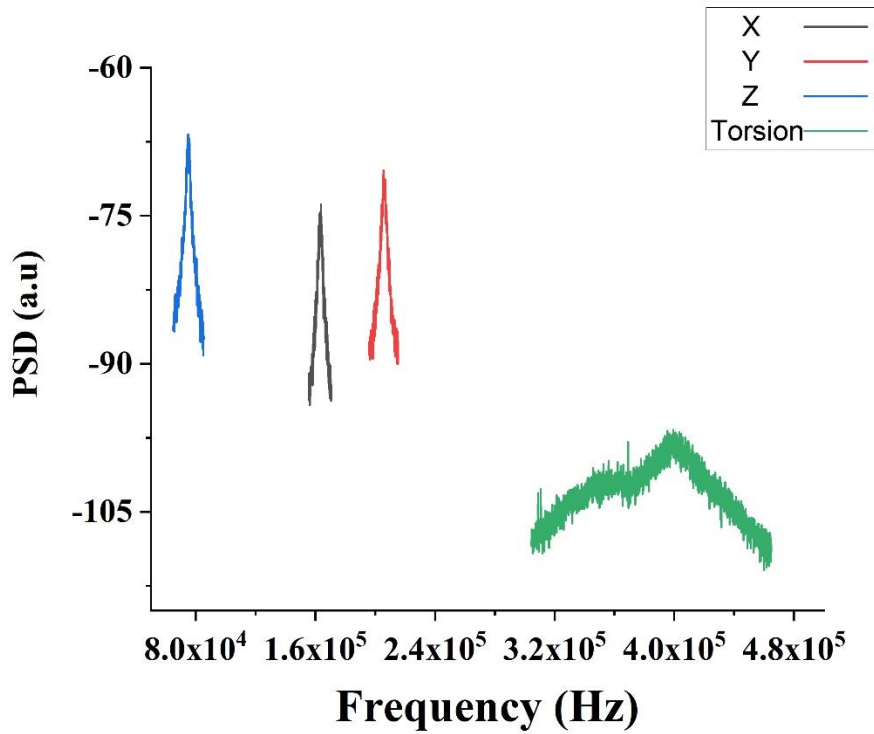
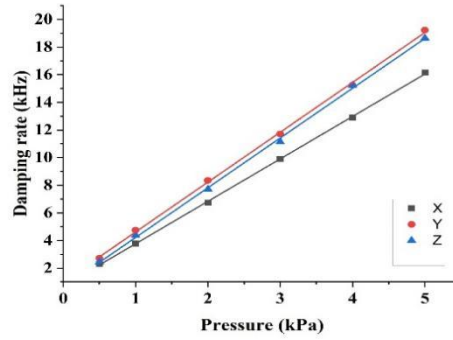


Figure 4.2: PSD of all three dimensions and PSD of torsional motion.

Torsional motion arises when the particles are not perfect spheres. The longest axis of the nanoparticle gets aligned along with the linear polarization due to the potential field^[68, 70, 77]. The frequency of torsional motion measured in our experiment is 350-400 kHz at a pressure of 500 Pa.

We use nonlinear fitting for CoM motion traces at different pressures. The associated damping rate for all three dimensions can be denoted by γ_x , γ_y and γ_z . The damping rate of nanoparticles of our experiment is given in Figure 4.3.

Figure 4.3: Damping rate of x , y , and z .

Once we have the damping rate of nanoparticles, we can use the damping rate formula from equation (2.12) to find out the size and mass of the nanoparticles. In our case, the measured length of particle in different directions are $x = 186$ nm, $y = 159$ nm and $z = 159$ nm. The length of all three sides is not equal, which clearly shows that the particle is not a perfect sphere. Now, we have all three sides of the nanoparticle, and now we can easily calculate the mass of the nanoparticle by using the density equation. The measured mass of the nanoparticle in our case is $m = 3.950 \times 10^{-17} \text{ kg}$.

4.3.3 Rotational motion without feedback cooling system

The experimental results are given in Figure 4.4. we observe the torsional motion and CoM motion of the nanoparticle at a pressure of about 500 Pa. Still, the rotation signal doesn't appear until the pressure reaches 100 Pa or below. When the pressure is high inside the chamber, the particle has very low damping rate and the amplitude of CoM motion is bigger which hides the rotation signal and can't be observed. Due to this reason, we can only observe the rotation signal at low pressure. The rotation and the CoM motion can influence each other, which leads to the coupling of the two motions. On the one hand, a large amplitude of the CoM motion causes a large change of the laser strength that the nanoparticle feels, and consequently induces a large fluctuation of the rotation frequency (the rotation frequency depends on the strength of the trapping laser). On the other hand, when rotation frequency is greater than CoM motion frequency and the fluctuation of the rotation frequency is greater than or equal to the CoM motion frequency, the energy of rotation can also be transferred to the CoM motion. Thus, the fluctuations of CoM and rotation motions are correlated. To measure the rotational motion, we change the

polarization of the trapping beam from linear to circular; after changing the polarization, torsional motion can't be observed. Simultaneously, we reduce the pressure through the mechanical pump while keeping the beam power constant at 300 mW and recording the traces with different pressure. In the beginning, we used a resistance gauge for the measurement of pressure, but its range is from 10^5 to 5×10^{-2} Pa. We use a hot cathode ionization gauge for further measurement, which is more trustable and gives us accurate results with a wide range from 0.2 Pa to 10^{-7} Pa. We have measured the beat signal of the nanoparticle's rotation at a frequency of 9.793 GHz shown in Figure 4.4(A) without a feedback cooling system. This is the $2f$ frequency, and the actual rotational frequency is about 4.8965 GHz at 0.12 Pa.

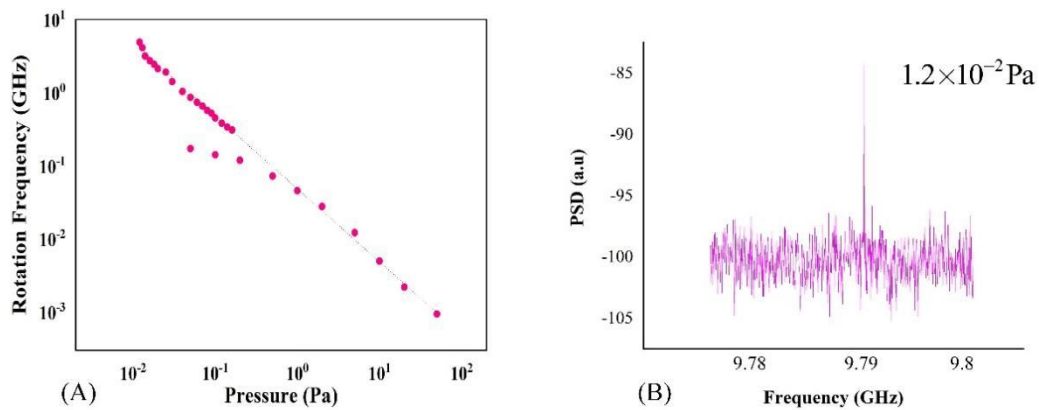


Figure 4.4: Measured rotational frequency of the nanoparticle and beat signal of the nanoparticle.

We can see a slight mismatch in rotation frequency given in Figure 4.4(A). Changing the pressure gauges cause this difference in traces of the measured frequency for the same particle. Figure 4.4(A) gives us a clear understanding of the relationship between pressure and rotation frequency. As we decrease the pressure, rotation frequency increases linearly and vice versa. At some point under a high vacuum, the nanoparticle doesn't follow the linear change in rotation frequency. The nanoparticle's frequency becomes nonlinear with a steeper slope, and can be explained with nonlinear elastodynamics. It's very easy to lose the particle in this region by reducing the pressure abruptly. The evacuation speed of the vacuum pump must be controlled with great care to achieve high rotation. But eventually, the nanoparticle is lost due to elastic nonlinearities. There is a limit in which the nonlinear rotation frequency reaches critical frequency. This case should be treated beyond nonlinear elastodynamics to determine the loss of nanoparticles from the optical trap^[75].

Figure 4.4(B). shows the beat signal of nanoparticle at pressure 1.2×10^{-2} Pa, the peak is at frequency of 9.8 GHz.

4.4 Conclusion

We optically trap a single nanoparticle using a high numerical aperture objective lens from atmospheric pressure to high vacuum by employing an experimental setup in the gravity direction without using a feedback cooling system. When the trapping laser beam is linearly polarized, we measure the center-of-motion motion with a balanced detection system and measure the torsional motion of the nanoparticle with a photodetector (Hamamatsu C12702-03). Torsional vibration of nanoparticles in the high vacuum can be used in detecting the Casimir torque and ultra-sensitive torque detection^[66, 77], and a step toward Cavendish torsion balance to study the quantum behavior of gravity^[78, 79]. By changing the linear polarization of the trapping beam to circular polarization, we detected a very high-speed rotation frequency (4.8965 GHz) of the nanoparticle with a high-speed fiber detector (New Focus 1554-A). These high-speed rotors can be used for an exclusive study of material properties and vacuum friction^[80-84].

Chapter 5: Interference of the scattered light from two optically levitated nanoparticles

5.1 Introduction

Young's double-slit experiment in physics is of great interest to understand the wave nature of light by observing the interference and diffraction like phenomena. It explains the wave-particle duality and has large-scale applications such as interferometry and precise measurement^[85-88]. As the trapping technique for ions and atoms developed, the faint scattered light interference from ions and atoms also have been reported ^[89, 90]. In most of the previous studies, they considered the field with the same polarization (i.e., scalar fields). More recently, the coherence of vector light fields in classical and quantum regimes became the new focus ^[91-94]. The polarization is considered in the complementarity principle and the coherence theorem. Young's double-slit interference irradiated by vector light fields has been realized and reported ^[89].

Optical levitation of micro and nano-particles by the radiation pressure of light field became an important platform for researchers since Ashkin's groundbreaking experiments with optical tweezers ^[6, 8]. Nanoparticles levitated in a vacuum have a very high Q-factor ^[58, 95], which can be used to detect weak force, precise measurement and even fundamental physics studies ^[31, 37, 62, 65, 96-98]. To cool the centre-of-mass motion of laser trapped nanoparticles to its quantum ground state was challenging, and many techniques have been proposed, like parametric feedback cooling^[40, 41, 99], speed feedback cooling^[39], cavity-assisting cooling ^[46], and electric feedback cooling ^[42-44]. The centre of mass motion of the trapped nanoparticles has been cooled to its quantum ground state recently^[48, 100, 101]. Optical levitation of nanoparticles offers an environment to measure the Casimir force^[66], torsional vibration of the nanoparticles ^[70, 77], and even to compute the GHz scale rotation of the particles, including the 6 GHz hyperfast rotation reported by our group ^[69, 70, 74, 77]. The optically levitated micro-and nano-particles system provides an environment free of particle-substrate interactions compared to those where the particles can interact with their surroundings ^[102, 103]. Our group recently published a paper about the experimental observation of dipole scattering from silica nanoparticles through an imaging system in the

Chapter 5: Interference of the scattered light from two optically levitated nanoparticles

Fourier space (k-space) and image space ^[104]. The dipole orientations of a single 3D molecule has been studied in detail by the polarization investigation of the emitted fluorescence ^[105-107], or aberrated ^[108], or by recording the defocused ^[102], or k-space ^[109-112]. In single-molecule imaging, the excitation laser illuminates the molecule confocally along the optical axis.

We experimentally examine the imaging and interference of the scattered vector light fields from two optically levitated nanoparticles in a single potential well. The system presented here has a few significant characteristics compared to those other systems where the particles-substrate interaction can't be ignored and has a notable influence on the scattered light. The environment is free of particle-substrate interactions in our system. In contrast, the excitation laser beam is being illuminated orthogonally to the optical axis of the objective lens. It has a dark background with a high signal-noise ratio while observing the dipole scattering.

Further on, when the optical axis of the objective lens and dipole orientation of nanoparticles align, the scattered vector light fields or polarization vortex can be produced. Two silica nanoparticles are trapped by two 1064 nm firmly focused laser beams having linear polarizations while the frequencies are different. Then we bring one beam through the motor-driving mirror near the second one to overlap and shift both the particles to a single potential well. Another 532 nm laser beam is used to illuminate the particles orthogonally. The scattered light of the nanoparticles is collected by the same objective and imaged on a high-resolution CCD. We observe the scattered light interference in image and Fourier space. This system can precisely determine the separation distance between the particles in a single potential well or separate potential wells.

Figure 5.1 shows the theoretical simulation of two nanoparticles in a single trapping laser beam. We have used a secondary 532 nm linearly polarized illuminating laser beam on the nanoparticles along the y-axis (perpendicular to the trapping beam). The wavelength of illuminating light is much larger than the size of nanoparticles, and particles can be regarded as dipoles.

5.2 Theoretical explanation

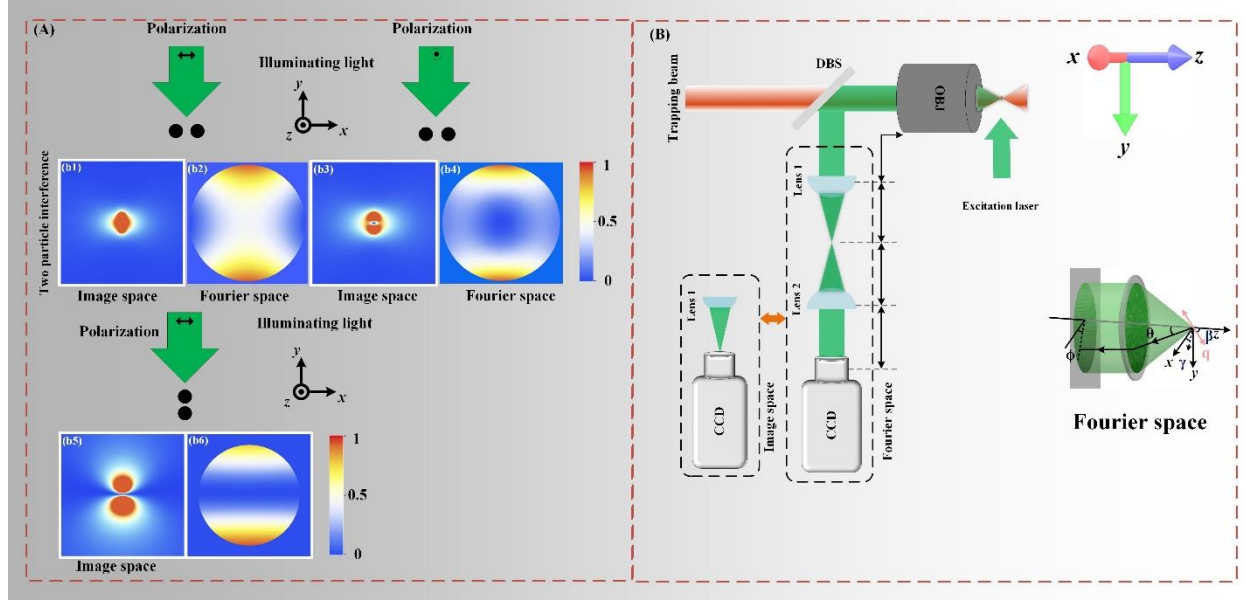


Figure 5.1. The schematic diagram of an imaging system and dipole scattering. (B) The diagram of an imaging system and trapping beam. The system can measure the dipole scattering in Fourier space with a 4f imaging system and image space. In (A), fig (b1), (b2), (b5) and (b6) represents the theoretical calculation for the intensity and polarization distribution of two nanoparticles in the image and Fourier space, while the excitation laser is along the x-axis. (b3) and (b4) image and Fourier space of two nanoparticles with the polarization of illuminating light along the z-axis. OBJ: objective lens; DBS: dichroic beam splitter.

Let's suppose a single particle in rectangular coordinates; the excitation laser induces dipole orientation. It can be denoted by (β, γ) (β (polar angle with respect to the z-axis), γ (azimuth angle in xy -plane with respect to the x-axis). Similarly, we can represent the scattering field vectors by (θ, φ) . The Fourier space (k-space) distribution of the scattering light which is the intensity distribution in the back aperture plane of the objective lens, can be written as^[104, 109]:

$$I^F(\theta, \varphi; \beta, \gamma) \propto \frac{1}{\cos\theta} (|q \cdot e_p|^2 + |q \cdot e_s|^2) \quad (5.1)$$

Where q represents the dipole orientation unit vector, i.e., $q = (\sin\beta \cos\gamma, \sin\beta \sin\gamma, \cos\beta)$, the unit vector e_p and e_s are orthogonal to each other. At the same time, both of them are perpendicular to the wave vector of the scattering field, defined as $e_p = (\cos\theta \cos\varphi, \cos\theta \sin\varphi, \sin\theta)$, $e_s = (\sin\varphi, -\cos\varphi, 0)$. The NA of the objective lens can determine the range of angle θ . In Fourier space, the polarization direction of the scattered light field can be

written as $p = (q \cdot e_p \cos\varphi + q \cdot e_s \sin\varphi, q \cdot e_p \sin\varphi - q \cdot e_s \cos\varphi)$, this spatial-dependent corresponds to the vector light field.

Here we will discuss two nanoparticles scattered light interference. let's consider the particles are line up along x -axis, i.e., $x_1 = -0.13\lambda$, $x_2 = 0.13\lambda$, as presented in Figure 5.1. The intensity distribution has been calculated from two dipoles in Fourier space. The intensity distribution interference of two linearly polarized light fields can be written as:

$$I_t^F(x^F, y^F) = I_1^F + I_2^F + 2\sqrt{I_1^F I_2^F} \cos\delta \cos\vartheta \quad (5.2)$$

Where δ and ϑ in Fourier space are spatial dependent. $\delta = k \left[\sqrt{r_1^2 + f^2} + \sqrt{r_2^2 + f^2} \right]$ are the phase difference and $\cos\vartheta = p_1 \cdot p_2 / |p_1| |p_2|$ is the intersection angle of polarization between the two light fields at a specific point, f is the focal length of the objective lens.

The intensity distribution in image space of the scattered light can be defined by the z component of the Poynting vector^[102, 113]:

$$I^I = \frac{c}{8\pi} e_z \cdot (\mathbf{E} \times \mathbf{B}) \quad (5.3)$$

the electric field \mathbf{E} and the magnetic field \mathbf{B} are defined as:

$$\begin{aligned} \mathbf{E} &= \iint m \sqrt{\frac{\cos\theta'}{\cos\theta}} [\mathbf{e}'_p(\mathbf{p} \cdot \mathbf{e}_p) + \mathbf{e}_s(\mathbf{p} \cdot \mathbf{e}_s)] e^{ik' \cdot r'} d\Omega \\ \mathbf{B} &= \iint m \sqrt{\frac{\cos\theta'}{\cos\theta}} [\mathbf{e}_s(\mathbf{p} \cdot \mathbf{e}_p) - \mathbf{e}'_p(\mathbf{p} \cdot \mathbf{e}_s)] e^{ik' \cdot r'} d\Omega \end{aligned} \quad (5.4)$$

where $d\Omega = \sin\theta' d\theta' d\varphi$, \mathbf{k}' and \mathbf{r}' are the wave vector and the position vector of the target point in image space, respectively. θ' is the intersection angle between \mathbf{k}' and z -axis. The relationship between θ and θ' is given by Abbe's sine condition, $\sin\theta = m \sin\theta'$, M is the magnification of the imaging system. The wave vector \mathbf{k}' and unit vector \mathbf{e}'_p can be defined as $\mathbf{k}' = 2\pi/\lambda (-\sin\theta' \cos\varphi, \sin\theta' \sin\varphi, -\cos\theta')$ and $\mathbf{e}'_p = (\cos\theta' \cos\varphi, \cos\theta' \sin\varphi, -\sin\theta')$, respectively. We can theoretically calculate the intensity and polarization distributions of scattered light of a single nanoparticle in the image and Fourier space according to Eq. (5.2) and (5.1), respectively.

We can calculate the interference distribution obtained from Eq. (5.4) in the image space. The complex amplitude form of the electric field in the image space (x, y) can be written as:

$$\mathbf{E}_j(x, y) = \frac{1}{r_j} \mathbf{p}_j e^{ikr_j} \quad (5.5)$$

where r_j is the distance between the field (x, y) and the position of the nanoparticle in the image space. The polarization of the scattered light fields $\mathbf{p}_j = (p_{xj}, p_{yj})$ can be resolved into x and y components. Thus the superposition of the two light fields in the image space (x, y) can be written as:

$$\begin{aligned} E_x &= \frac{1}{r_1} p_{x1} e^{ikr_1} + \frac{1}{r_2} p_{x2} e^{ikr_2} \\ E_y &= \frac{1}{r_1} p_{y1} e^{ikr_1} + \frac{1}{r_2} p_{y2} e^{ikr_2} \end{aligned} \quad (5.6)$$

The polarization of illuminating light will be considered for three cases along the x - and z -axis. Case 1: $(\beta, \gamma) = (0, 0)$, in this case, the linearly polarized illuminating light is along the x -axis, and the two nanoparticles are trapped in the y -axis of the trapping beam. The scattered light intensity and polarization distribution are given in Fig. 5.1(A). In the image space, the intensity distribution represents an elliptical geometric shape Fig. 5.1(A(b1)), and its corresponding Fourier transform is also shown in Fig. 5.1(A(b2)). Case 2: $(\beta, \gamma) = (\pi/2, 0)$, in this case, the linearly polarized illuminating beam has been rotated by $\pi/2$ radians, and the polarization is along the z -axis while particles are in the y -axis of the trapping beam. The scattered light intensity distribution has been changed into a donut hole in the image space Fig. 5.1(A(b3)) and in Fourier space as well Fig. 5.1(A(b4)). Case 3: $(\beta, \gamma) = (0, 0)$, now, in this case, the trapping beam has been rotated, and the particles are in the x -axis of the trapping beam. The illuminating light hits both the particles, and the intensity and polarization distribution of two dipoles can be observed in image and Fourier space. Both the particles have a minimal distance in between and can be regarded as two dipole nano-antennas with the same phase; in Fourier space images, we can observe a dark dull separation in the middle.

5.3 Experiment

The schematic design of our experimental setup is shown in Fig. 5.2. In the beginning, we have used two 1064 nm linearly polarized laser beams generated by (20W,

Chapter 5: Interference of the scattered light from two optically levitated nanoparticles

CW, DPSS FG-VIB) laser having TEM_{00} Gaussian mode in the gravity direction to optically trapped two silica nanoparticles in each potential well. We have used an AOM to shift the frequency of one beam by a amount of 110 MHz. The shifted and un-shifted laser beams are combined through PBS and then pass through the quarter and half-wave plates.

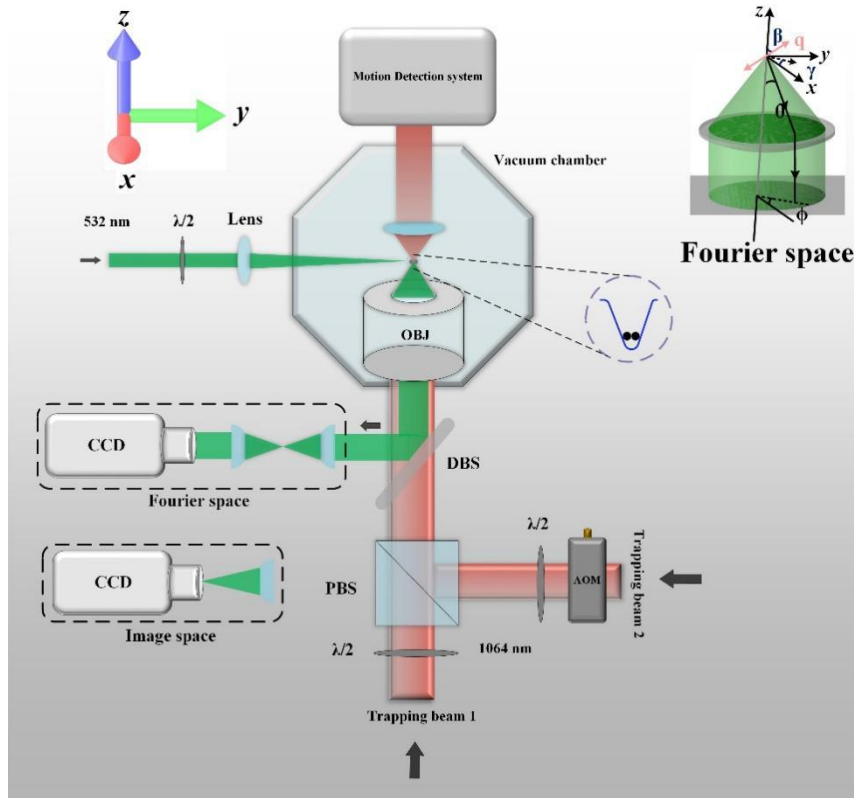


FIG. 5.2. Schematic diagram of our experimental setup. Two trapping beams with a different frequency are tightly focused by a high NA objective lens ($NA=0.95$) to trap two nanoparticles and then make them together by bringing one beam near another. Another 532 nm laser beam illuminates the nanoparticles perpendicularly, while the same objective collects the scattered light and imaged it on a CCD. The trapping beam output light can be used to detect the motion of particles. DBS: dichroic beam splitter; PBS: polarizing beam splitter; AOM: acousto-optic modulator; $\lambda/2$: half-wave plate.

We have kept the power of both trapping beams of about 245 mW. The trapping beams are propagating on the z-axis. The polarization of the trapping beams can be adjusted according to the experimental requirements. An objective lens tightly focuses the vertically propagating trapping beams with a high numerical aperture ($NA= 0.95$) in the vacuum chamber. The working distance of the objective is 0.3 mm. We use another high NA aspheric lens ($NA= 0.68$) to collect the trapping beam's output light to detect the CoM

motion signal of nanoparticles with a balanced detection system. One beam is precisely controlled by Pico-motor (New focus) to move the beam to any desired location within the objective plan. The distance between the two potential wells in the axial can be adjusted by changing the position of the trapping beam. In our experiment, we have used the commercial silica nanoparticles of diameter 177 nm whose dispersion is low enough. The silica nanoparticles are hydrosoluble, which are first dissolved in very pure ethanol at a concentration of about $1.2 \times 10^{10}/\text{ml}$ and then sonicated for at least 30 minutes. The diluted nanoparticles are then poured manually into an ultrasonic nebulizer. The liquid which contains the droplets of nanoparticles is then dispersed with the help of a nebulizer and directed by a thin and long narrow tube into the focus region of the objective in the chamber. At the start, we keep the distance between the two potential wells to about $4\mu\text{m}$ for trapping two single nanoparticles. When a single potential well traps a nanoparticle, we decrease the pouring speed to avoid losing the trapped particle due to air flow. Once the two single nanoparticles get trapped in two potentials individually, then we stop the pouring and close the chamber. We use the motor driving mirror to bring one particle closer to another. As the two potential wells overlap and both the particles shift to one potential well, we block the other beam, and two nanoparticles get trapped in a single potential well.

Another 532 nm linearly polarized laser beam passes through a half-wave plate and is then focused by a spherical lens ($f=175\text{ mm}$) to illuminate the two optically trapped nanoparticles. We can adjust the direction of linear polarization through a half-wave plate. The propagating direction of illuminating laser is along the y -axis, which is orthogonal to the direction (z -axis) of the trapping laser. The illuminating laser beam waist is about $50\mu\text{m}$ at the position of nanoparticles, which is larger than the separation and displacement between the two trapped nanoparticles. We have kept the power of illuminating beam about $100\mu\text{W}$, which has negligible influence on the nanoparticle's motion and can be neglected. The nanoparticles sizes are tiny compared to the wavelength of illuminating laser beam; therefore, we can treat the two nanoparticles as two dipoles. The same objective lens collects the scattered light from two nanoparticles, then reflected by a dichroic mirror (532 HR and 1064 AR) and imaged on a CCD camera (Andor Zyla

eCMOS). We measure the scattered light in image space and Fourier space with the help of a 4f imaging system.

5.4 Results and discussion

This article focuses on the scattered light interference from two nanoparticles trapped in a single potential well. Our group previously studied the intensity and polarization distribution in detail^[104]. We have observed the scattered light interference from two nanoparticles in image and Fourier space. In the first case, we have observed the interference of scattered light when the input linear polarization of illuminating light has different directions, as shown in Fig.5.3. The illuminating light propagating in the y-direction and the two nanoparticles are also trapped in the y-axis of the trapping beam. The two nanoparticles behave like a single particle in Fig. 5.3 (a2) -(g2). The linear polarization of the illuminating light is along the x-axis perpendicular to the optical axis of the objective. The illuminating light only hits and single particle and behaves like a single dipole. Now, when we rotate the polarization of illuminating light in xz -plane anti-clockwise, every $\pi/6$ radian and the scattered light images are recorded in Fourier space (Fig. 5.3(a3) -(g3)) and image space (Fig. 5.3(a2) -(g2)). When the dipole orientation gets adjusted along the z-axis, the intensity distribution presents a pattern like donut hole for the scattered light and displays a vector light with radial polarization. In the second case, we rotate the trapping beam, and the nanoparticles rotate in the optical axis. In this case, the nanoparticles are in the x-axis of the trapping beam, and the illuminating beam propagates along the y-axis, which hits both the particles and we can observe the two dipoles scattered light in image space Fig. 5.3(a5) -(g5) and in Fourier space Fig. 5.3(a6) -(g6) respectively. We can see the separation distance between the two nanoparticles, like two dipoles nano-antennas with the same phase, and we can observe a dark dull separation (marked in brown dashed lines). When the illuminating light is rotated in the xz -plane, and linear polarization becomes aligned along the z-axis, the intensity distribution shows two donut holes overlapping. Fourier space also presents a donut like structure (empty in the middle) overlapping the dark dull separation.

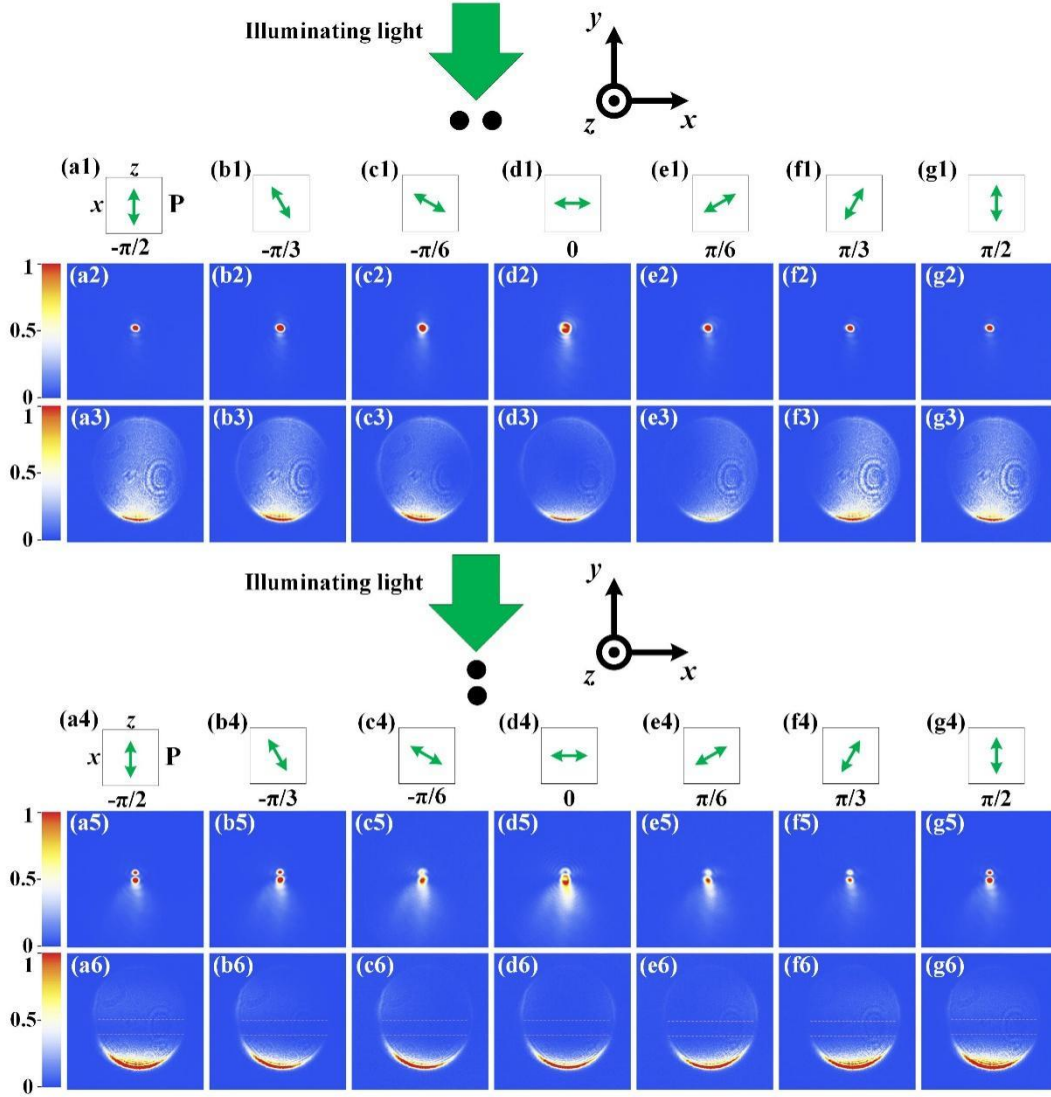


FIG. 5.3. The images of two particles scattered light interference with respect to linear polarization of illuminating laser in image and Fourier space. (a1) -(g1) and (a4) -(g4) represents the illuminating beam polarization. (a2) -(g2) are image space results for one case, and (a3) -(g3) are their Fourier space results. (a5) -(g5) are 2nd case image space results, and (a6) -(g6) are their Fourier space results. The trapping beam polarization is along y -axis for (a2) -(g2) and (a3) -(g3) while for (a5) -(g5) and (a6) -(g6) it has been kept in the x -axis.

In Fig.5.4, the interference of scattered light from two nanoparticles has been observed in image space and Fourier space by keeping the linearly polarized illuminating light at a specific direction and rotating the trapping beam counter-clockwise in the xy -plane. In the first case, the linearly polarized illuminating beam is aligned along the x -axis perpendicular to the optical axis of the objective while propagating in the y -direction. The

two nanoparticles are trapped in the y -axis of the trapping beam, and only the single particle gets exposed to the illuminating beam.

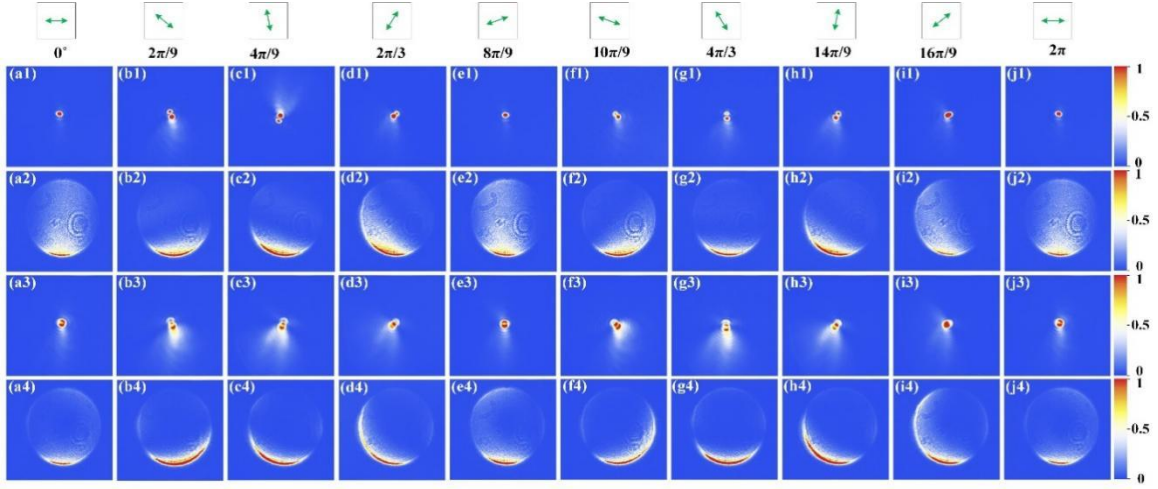


Figure 5.4. The scattered light interference images for different directions of the linearly polarized trapping beam and illuminating light in Fourier and image space. In (a1) -(j1), the linearly polarized illuminating light is along the x -axis, and the trapping beam has been rotated 2π (a2) -(j2) are their corresponding Fourier images. In (a3) -(j3), the illuminating beam is along the z -axis, and (a4) -(j4) are the corresponding Fourier space images. The linearly polarized illuminating beam polarization is along x -axis for (a1) -(j1) and (a2) -(j2) while for (a3) -(j3) and (a4) -(j4) it has been kept in the z -axis.

Now, we rotate the trapping beam every $2\pi/9$ radian; we rotate the angle by this rate to cover the whole 2π circle and it's hard to include each angle in the thesis while the results have been recorded in image space Fig. 5.4(a1) -(j1) and Fourier space Fig. 5.4(a2) -(j2). We can observe the distance between the two nanoparticles in image space while rotating the trapping beam and a dark dull separation in the middle of Fourier space images. In the second case, we adjust the linearly polarized illuminating beam along the z -axis while propagating in the y -direction. Now, we rotate the trapping beam every $2\pi/9$ radian; the results have been recorded in image space Fig. 5.4(a3) -(j3) and Fourier space Fig.5.4(a4) -(j4).

Note: Note: the scattered light in the forward direction is stronger than the backward direction in our experiment, clearly visible in figure 5.3 and figure 5.4.

5.5 Summary

We have observed the interference of two scattered vector light fields for different polarization of the illuminating light and trapping beam. The two nanoparticles are optically levitated in a single potential well with a separation distance of about 0.26λ . The system presented here have a few distinguishing features like free of particle-substrate interactions and have a dark background with a high signal-noise ratio while observing the dipole scattering. Further on, when the optical axis of the objective lens and dipole orientation of nanoparticles align, the scattered vector light fields or polarization vortex can be produced. It can be used as two dipole nano-antennas with the same phase. Furthermore, the diffraction of optical elements causes the Rayleigh diffraction rings, which were also detected. This system can be used to study the dynamical properties, scattering anisotropy, near-field optics, optical trapping and imaging.

References

- [1] Kepler J. De cometis libelli tres ... De cometis libelli tres. Typis Andreae Apergeri, sumptibus Sebastiani Mylii bibliopolæ Augustani[J]. 1619.
- [2] Maxwell J C. A treatise on electricity and magnetism. De cometis libelli tres.Dover[J]. 1891, 1873.
- [3] Lebedew P. Untersuchungen über die Druckkräfte des Lichtes[J]. 1901, 311(11): 433-458.
- [4] Nichols E F, Hull G F. A Preliminary Communication on the Pressure of Heat and Light Radiation[J]. Physical Review (Series I), 1901, 13(5): 307-320.
- [5] Townes C H. How the laser happened: adventures of a scientist / Charles H. Townes[J]. Oxford University Press New York, 1999.
- [6] Ashkin A. Acceleration and Trapping of Particles by Radiation Pressure[J]. Physical Review Letters, 1970, 24(4): 156-159.
- [7] Ashkin A, Dziedzic J M. Optical Levitation by Radiation Pressure[J]. 1971, 19(8): 283-285.
- [8] Ashkin A, Dziedzic J M. Optical levitation in high vacuum[J]. 1976, 28(6): 333-335.
- [9] Ashkin A, Dziedzic J M. Feedback stabilization of optically levitated particles[J]. 1977, 30(4): 202-204.
- [10] Ashkin A, Dziedzic J M. Optical Trapping and Manipulation of Viruses and Bacteria[J]. 1987, 235(4795): 1517-1520.
- [11] Ashkin A. Forces of a single-beam gradient laser trap on a dielectric sphere in the ray optics regime[J]. Methods Cell Biol, 1998, 55: 1–27
- [12] Grier D G. A revolution in optical manipulation[J]. Nature, 2003, 424(6950): 810-816.
- [13] Mishchenko M I J J o Q S, Transfer R. Optical Tweezers: Principles and Applications, P.H. Jones, O.M. Maragò, G. Volpe. Cambridge University Press, Cambridge, UK (2015). xvi+547 pp., Hardbound, ISBN: 978-1-107-05116-4[J]. 2016, 179: 217.
- [14] Ashkin A, Dziedzic J M, Bjorkholm J E, et al. Observation of a single-beam gradient force optical trap for dielectric particles[J]. Optics Letters, 1986, 11(5): 288-290.

References

- [15] Wright W H, Sonek G J, Berns M W. Parametric study of the forces on microspheres held by optical tweezers[J]. *Applied Optics*, 1994, 33(9): 1735-1748.
- [16] Harada Y, Asakura T. Radiation forces on a dielectric sphere in the Rayleigh scattering regime[J]. *Optics Communications*, 1996, 124(5): 529-541.
- [17] Nieminen T A, Loke V L Y, Stilgoe A B, et al. Optical tweezers computational toolbox[J]. *Journal of Optics A: Pure and Applied Optics*, 2007, 9(8): S196-S203.
- [18] MATLAB functions for Mie scattering and absorption[J].
- [19] S. Yushmanov J S C, and K. C. Koppenhoefer. Mie scattering of electromagnetic waves[J]. 2013.
- [20] Lock J A, Gouesbet G. Generalized Lorenz–Mie theory and applications[J]. *Journal of Quantitative Spectroscopy and Radiative Transfer*, 2009, 110(11): 800-807.
- [21] Pesce G, Jones P H, Maragò O M, et al. Optical tweezers: theory and practice[J]. *The European Physical Journal Plus*, 2020, 135(12): 949.
- [22] Brown R. XXVII. A brief account of microscopical observations made in the months of June, July and August 1827, on the particles contained in the pollen of plants; and on the general existence of active molecules in organic and inorganic bodies[J]. *The Philosophical Magazine*, 1828, 4(21): 161-173.
- [23] Einstein A. Über die von der molekularkinetischen Theorie der Wärme geforderte Bewegung von in ruhenden Flüssigkeiten suspendierten Teilchen[J]. 1905, 322(8): 549-560.
- [24] Li T, Kheifets S, Medellin D, et al. Measurement of the Instantaneous Velocity of a Brownian Particle[J]. *Science*, 2010, 328(5986): 1673-1675.
- [25] Uhlenbeck G E, Ornstein L S. On the Theory of the Brownian Motion[J]. *Physical Review*, 1930, 36(5): 823-841.
- [26] Wang M C, Uhlenbeck G E. On the Theory of the Brownian Motion II[J]. *Reviews of Modern Physics*, 1945, 17(2-3): 323-342.
- [27] Nørrelykke S F, Flyvbjerg H. Harmonic oscillator in heat bath: Exact simulation of time-lapse-recorded data and exact analytical benchmark statistics[J]. *Physical Review E*, 2011, 83(4): 041103.
- [28] Berg-Sørensen K, Flyvbjerg H. Power spectrum analysis for optical tweezers[J]. 2004, 75(3): 594-612.

References

- [29] Beresnev S A, Chernyak V G, Fomyagin G A. Motion of a spherical particle in a rarefied gas. Part 2. Drag and thermal polarization[J]. *Journal of Fluid Mechanics*, 1990, 219: 405-421.
- [30] Hebestreit E, Reimann R, Frimmer M, et al. Measuring the internal temperature of a levitated nanoparticle in high vacuum[J]. *Physical Review A*, 2018, 97(4): 043803.
- [31] Hebestreit E, Frimmer M, Reimann R, et al. Sensing Static Forces with Free-Falling Nanoparticles[J]. *Physical Review Letters*, 2018, 121(6): 063602.
- [32] Romero-Isart O, Juan M L, Quidant R, et al. Toward quantum superposition of living organisms[J]. *New Journal of Physics*, 2010, 12(3): 033015.
- [33] Poggio M, Degen C L, Mamin H J, et al. Feedback Cooling of a Cantilever's Fundamental Mode below 5 mK[J]. *Physical Review Letters*, 2007, 99(1): 017201.
- [34] Bassi A, Lochan K, Satin S, et al. Models of wave-function collapse, underlying theories, and experimental tests[J]. *Reviews of Modern Physics*, 2013, 85(2): 471-527.
- [35] Romero-Isart O, Pflanzner A C, Juan M L, et al. Optically levitating dielectrics in the quantum regime: Theory and protocols[J]. *Physical Review A*, 2011, 83(1): 013803.
- [36] Bateman J, Nimmrichter S, Hornberger K, et al. Near-field interferometry of a free-falling nanoparticle from a point-like source[J]. *Nature Communications*, 2014, 5(1): 4788.
- [37] Geraci A A, Papp S B, Kitching J. Short-Range Force Detection Using Optically Cooled Levitated Microspheres[J]. *Physical Review Letters*, 2010, 105(10): 101101.
- [38] Manjavacas A, García de Abajo F J. Vacuum Friction in Rotating Particles[J]. *Physical Review Letters*, 2010, 105(11): 113601.
- [39] Li T, Kheifets S, Raizen M G. Millikelvin cooling of an optically trapped microsphere in vacuum[J]. *Nature Physics*, 2011, 7(7): 527-530.
- [40] Gieseler J, Deutsch B, Quidant R, et al. Subkelvin Parametric Feedback Cooling of a Laser-Trapped Nanoparticle[J]. *Physical Review Letters*, 2012, 109(10): 103603.
- [41] Vovrosh J, Rashid M, Hempston D, et al. Parametric feedback cooling of levitated optomechanics in a parabolic mirror trap[J]. *Journal of the Optical Society of America B*, 2017, 34(7): 1421-1428.
- [42] Iwasaki M, Yotsuya T, Naruki T, et al. Electric feedback cooling of single charged nanoparticles in an optical trap[J]. *Physical Review A*, 2019, 99(5): 051401.

References

- [43] Conangla G P, Ricci F, Cuairan M T, et al. Optimal Feedback Cooling of a Charged Levitated Nanoparticle with Adaptive Control[J]. *Physical Review Letters*, 2019, 122(22): 223602.
- [44] Tebbenjohanns F, Frimmer M, Militaru A, et al. Cold Damping of an Optically Levitated Nanoparticle to Microkelvin Temperatures[J]. *Physical Review Letters*, 2019, 122(22): 223601.
- [45] Delić U, Reisenbauer M, Grass D, et al. Cavity Cooling of a Levitated Nanosphere by Coherent Scattering[J]. *Physical Review Letters*, 2019, 122(12): 123602.
- [46] Windey D, Gonzalez-Ballester C, Maurer P, et al. Cavity-Based 3D Cooling of a Levitated Nanoparticle via Coherent Scattering[J]. *Physical Review Letters*, 2019, 122(12): 123601.
- [47] Meyer N, Sommer A d I R, Mestres P, et al. Resolved-Sideband Cooling of a Levitated Nanoparticle in the Presence of Laser Phase Noise[J]. *Physical Review Letters*, 2019, 123(15): 153601.
- [48] Delić U, Reisenbauer M, Dare K, et al. Cooling of a levitated nanoparticle to the motional quantum ground state[J]. *Science*, 2020, 367(6480): 892-895.
- [49] Moser J, Güttinger J, Eichler A, et al. Ultrasensitive force detection with a nanotube mechanical resonator[J]. *Nature Nanotechnology*, 2013, 8(7): 493-496.
- [50] Rademacher M, Millen J, Li Y L. Quantum sensing with nanoparticles for gravimetry: when bigger is better %J *Advanced Optical Technologies*[J]. 2020, 9(5): 227-239.
- [51] Rashid M, Toroš M, Setter A, et al. Precession Motion in Levitated Optomechanics[J]. *Physical Review Letters*, 2018, 121(25): 253601.
- [52] Chaste J, Eichler A, Moser J, et al. A nanomechanical mass sensor with yoctogram resolution[J]. *Nature Nanotechnology*, 2012, 7(5): 301-304.
- [53] Ricci F, Cuairan M T, Conangla G P, et al. Accurate Mass Measurement of a Levitated Nanomechanical Resonator for Precision Force-Sensing[J]. *Nano Letters*, 2019, 19(10): 6711-6715.
- [54] Blakemore C P, Rider A D, Roy S, et al. Precision Mass and Density Measurement of Individual Optically Levitated Microspheres[J]. *Physical Review Applied*, 2019, 12(2): 024037.
- [55] Cleland A N, Roukes M L. A nanometre-scale mechanical electrometer[J]. *Nature*, 1998, 392(6672): 160-162.

References

- [56] Ohlinger A, Deak A, Lutich A A, et al. Optically Trapped Gold Nanoparticle Enables Listening at the Microscale[J]. *Physical Review Letters*, 2012, 108(1): 018101.
- [57] Millen J, Deesuwat T, Barker P, et al. Nanoscale temperature measurements using non-equilibrium Brownian dynamics of a levitated nanosphere[J]. *Nature Nanotechnology*, 2014, 9(6): 425-429.
- [58] YIN Z-Q, GERACI A A, LI T. OPTOMECHANICS OF LEVITATED DIELECTRIC PARTICLES[J]. 2013, 27(26): 1330018.
- [59] Norte R A, Moura J P, Gröblacher S. Mechanical Resonators for Quantum Optomechanics Experiments at Room Temperature[J]. *Physical Review Letters*, 2016, 116(14): 147202.
- [60] Purdy T P, Peterson R W, Yu P L, et al. Cavity optomechanics with Si₃N₄ membranes at cryogenic temperatures[J]. *New Journal of Physics*, 2012, 14(11): 115021.
- [61] Ricci F, Rica R A, Spasenović M, et al. Optically levitated nanoparticle as a model system for stochastic bistable dynamics[J]. *Nature Communications*, 2017, 8(1): 15141.
- [62] Jain V, Gieseler J, Moritz C, et al. Direct Measurement of Photon Recoil from a Levitated Nanoparticle[J]. *Physical Review Letters*, 2016, 116(24): 243601.
- [63] Omori R, Kobayashi T, Suzuki A. Observation of a single-beam gradient-force optical trap for dielectric particles in air[J]. *Opt Lett*, 1997, 22(11): 816-818.
- [64] Conangla G P, Schell A W, Rica R A, et al. Motion Control and Optical Interrogation of a Levitating Single Nitrogen Vacancy in Vacuum[J]. *Nano Letters*, 2018, 18(6): 3956-3961.
- [65] Winstone G, Bennett R, Rademacher M, et al. Direct measurement of the electrostatic image force of a levitated charged nanoparticle close to a surface[J]. *Physical Review A*, 2018, 98(5): 053831.
- [66] Xu Z, Li T. Detecting Casimir torque with an optically levitated nanorod[J]. *Physical Review A*, 2017, 96(3): 033843.
- [67] Shao L, Andr n D, Jones S, et al. Optically controlled stochastic jumps of individual gold nanorod rotary motors[J]. *Physical Review B*, 2018, 98(8): 085404.
- [68] Hoang T M, Ma Y, Ahn J, et al. Torsional Optomechanics of a Levitated Nonspherical Nanoparticle[J]. *Physical Review Letters*, 2016, 117(12): 123604.
- [69] Jin Y, Yan J, Rahman S J, et al. 600;GHz hyperfast rotation of an optically levitated nanoparticle in vacuum[J]. *Photonics Research*, 2021, 9(7): 1344-1350.

References

- [70] Ahn J, Xu Z, Bang J, et al. Optically Levitated Nanodumbbell Torsion Balance and GHz Nanomechanical Rotor[J]. *Physical Review Letters*, 2018, 121(3): 033603.
- [71] La Porta A, Wang M D. Optical Torque Wrench: Angular Trapping, Rotation, and Torque Detection of Quartz Microparticles[J]. *Physical Review Letters*, 2004, 92(19): 190801.
- [72] Kuhn S, Stickler B A, Kosloff A, et al. Optically driven ultra-stable nanomechanical rotor[J]. *Nature Communications*, 2017, 8(1): 1670.
- [73] Monteiro F, Ghosh S, van Assendelft E C, et al. Optical rotation of levitated spheres in high vacuum[J]. *Physical Review A*, 2018, 97(5): 051802.
- [74] Reimann R, Doderer M, Hebestreit E, et al. GHz Rotation of an Optically Trapped Nanoparticle in Vacuum[J]. *Physical Review Letters*, 2018, 121(3): 033602.
- [75] Hümmer D, Lampert R, Kustura K, et al. Acoustic and optical properties of a fast-spinning dielectric nanoparticle[J]. *Physical Review B*, 2020, 101(20): 205416.
- [76] Fremerey J K. Spinning rotor vacuum gauges[J]. *Vacuum*, 1982, 32(10): 685-690.
- [77] Ahn J, Xu Z, Bang J, et al. Ultrasensitive torque detection with an optically levitated nanorotor[J]. *Nature Nanotechnology*, 2020, 15(2): 89-93.
- [78] Marletto C, Vedral V. Gravitationally Induced Entanglement between Two Massive Particles is Sufficient Evidence of Quantum Effects in Gravity[J]. *Physical Review Letters*, 2017, 119(24): 240402.
- [79] Bose S, Mazumdar A, Morley G W, et al. Spin Entanglement Witness for Quantum Gravity[J]. *Physical Review Letters*, 2017, 119(24): 240401.
- [80] Schuck M, Steinert D, Nussbaumer T, et al. Ultrafast rotation of magnetically levitated macroscopic steel spheres[J]. 2018, 4(1): e1701519.
- [81] Nagornykh P, Coppock J E, Murphy J P J, et al. Optical and magnetic measurements of gyroscopically stabilized graphene nanoplatelets levitated in an ion trap[J]. *Physical Review B*, 2017, 96(3): 035402.
- [82] Zhao R, Manjavacas A, García de Abajo F J, et al. Rotational Quantum Friction[J]. *Physical Review Letters*, 2012, 109(12): 123604.
- [83] Guo Y, Jacob Z. Giant non-equilibrium vacuum friction: role of singular evanescent wave resonances in moving media[J]. *Journal of Optics*, 2014, 16(11): 114023.
- [84] Manjavacas A, Rodríguez-Fortuño F J, García de Abajo F J, et al. Lateral Casimir Force on a Rotating Particle near a Planar Surface[J]. *Physical Review Letters*, 2017, 118(13): 133605.

References

- [85] Eichmann U, Bergquist J C, Bollinger J J, et al. Young's interference experiment with light scattered from two atoms[J]. *Physical Review Letters*, 1993, 70(16): 2359-2362.
- [86] Wootters W K, Zurek W H. Complementarity in the double-slit experiment: Quantum nonseparability and a quantitative statement of Bohr's principle[J]. *Physical Review D*, 1979, 19(2): 473-484.
- [87] Englert B-G. Fringe Visibility and Which-Way Information: An Inequality[J]. *Physical Review Letters*, 1996, 77(11): 2154-2157.
- [88] Sanz Á S, Miret-Artés S, *Interference and Interferometry, A Trajectory Description of Quantum Processes. II. Applications: A Bohmian Perspective*, Springer Berlin Heidelberg, Berlin, Heidelberg, 2014, pp. 97-133.
- [89] Grangier P, Aspect A, Vigue J. Quantum Interference Effect for Two Atoms Radiating a Single Photon[J]. *Physical Review Letters*, 1985, 54(5): 418-421.
- [90] Wolf S, Wechs J, von Zanthier J, et al. Visibility of Young's Interference Fringes: Scattered Light from Small Ion Crystals[J]. *Physical Review Letters*, 2016, 116(18): 183002.
- [91] Gori F, Santarsiero M, Borghi R. Vector mode analysis of a Young interferometer[J]. *Optics Letters*, 2006, 31(7): 858-860.
- [92] Eberly J H, Qian X F, Vamivakas A N. Polarization coherence theorem[J]. *Optica*, 2017, 4(9): 1113-1114.
- [93] Norrman A, Blomstedt K, Setälä T, et al. Complementarity and Polarization Modulation in Photon Interference[J]. *Physical Review Letters*, 2017, 119(4): 040401.
- [94] Qian X F, Agarwal G S. Quantum duality: A source point of view[J]. *Physical Review Research*, 2020, 2(1): 012031.
- [95] J. Millen T S M, R. Pettit, and A. N. Vamivakas. Optomechanics with levitated particles[J]. *Rep. Prog. Phys*, 2020, 83: 026401.
- [96] Ranjit G, Atherton D P, Stutz J H, et al. Attonewton force detection using microspheres in a dual-beam optical trap in high vacuum[J]. *Physical Review A*, 2015, 91(5): 051805.
- [97] Aspelmeyer M, Kippenberg T J, Marquardt F. Cavity optomechanics[J]. *Reviews of Modern Physics*, 2014, 86(4): 1391-1452.
- [98] Arndt M, Hornberger K. Testing the limits of quantum mechanical superpositions[J]. *Nature Physics*, 2014, 10(4): 271-277.

References

- [99] Zheng Y, Guo G-C, Sun F-W. Cooling of a levitated nanoparticle with digital parametric feedback[J]. 2019, 115(10): 101105.
- [100] Tebbenjohanns F, Mattana M L, Rossi M, et al. Quantum control of a nanoparticle optically levitated in cryogenic free space[J]. *Nature*, 2021, 595(7867): 378-382.
- [101] Magrini L, Rosenzweig P, Bach C, et al. Real-time optimal quantum control of mechanical motion at room temperature[J]. *Nature*, 2021, 595(7867): 373-377.
- [102] Böhmer M, Enderlein J. Orientation imaging of single molecules by wide-field epifluorescence microscopy[J]. *Journal of the Optical Society of America B*, 2003, 20(3): 554-559.
- [103] Zhou H, Qin C, Chen R, et al. Quantum Coherent Modulation-Enhanced Single-Molecule Imaging Microscopy[J]. *The Journal of Physical Chemistry Letters*, 2019, 10(2): 223-228.
- [104] Jin Y, Yan J, Rahman S J, et al. Imaging the dipole scattering of an optically levitated dielectric nanoparticle[J]. 2021, 119(2): 021106.
- [105] Fourkas J T. Rapid determination of the three-dimensional orientation of single molecules[J]. *Optics Letters*, 2001, 26(4): 211-213.
- [106] Zhanghao K, Chen X, Liu W, et al. Super-resolution imaging of fluorescent dipoles via polarized structured illumination microscopy[J]. *Nature Communications*, 2019, 10(1): 4694.
- [107] Lethiec C, Laverdant J, Vallon H, et al. Measurement of Three-Dimensional Dipole Orientation of a Single Fluorescent Nanoemitter by Emission Polarization Analysis[J]. *Physical Review X*, 2014, 4(2): 021037.
- [108] Bartko A P, Dickson R M. Three-Dimensional Orientations of Polymer-Bound Single Molecules[J]. *The Journal of Physical Chemistry B*, 1999, 103(16): 3053-3056.
- [109] Lieb M A, Zavislan J M, Novotny L. Single-molecule orientations determined by direct emission pattern imaging[J]. *Journal of the Optical Society of America B*, 2004, 21(6): 1210-1215.
- [110] Dodson C M, Kurvits J A, Li D, et al. Wide-angle energy-momentum spectroscopy[J]. *Optics Letters*, 2014, 39(13): 3927-3930.
- [111] Osorio C I, Mohtashami A, Koenderink A F. K-space polarimetry of bullseye plasmon antennas[J]. *Scientific Reports*, 2015, 5(1): 9966.

References

- [112] Curcio V, Alemán-Castañeda L A, Brown T G, et al. Birefringent Fourier filtering for single molecule coordinate and height super-resolution imaging with dithering and orientation[J]. Nature Communications, 2020, 11(1): 5307.
- [113] Enderlein J. Theoretical study of detection of a dipole emitter through an objective with high numerical aperture[J]. Optics Letters, 2000, 25(9): 634-636.

Research achievements

- [1]. Yuanbin Jin, Jiangwei Yan, **Shah Jee Rahman**, Jie Li, Xudong, and Jing Zhang. 6 GHz hyperfast rotation of an optically levitated nanoparticle in vacuum, *Photonic Research*. 9, 1344 (2021).
- [2]. Yuanbin Jin, Jiangwei Yan, **Shah Jee Rahman**, Xudong, and Jing Zhang. Imaging the dipole scattering of an optically levitated dielectric nanoparticle, *Applied Physics Letter*. 119, 021106 (2021).
- [3]. Yuanbin Jin, Jiangwei Yan, **Shah Jee Rahman**, Xudong, and Jing Zhang. Interference of the scattered vector light fields from two optically levitated nanoparticles. (Accepted in *optics express*)

Acknowledgments

Acknowledgments

First of all, I would like to thank Professor Zhang Jing for giving me the opportunity to work in such a tremendous and well-reputed lab. I am very impressed by his confidence, creativity and attitude doing research. I have seen him working hard day and night. Back in my country, often we thought about how China developed so fast! In these three years, I have witnessed the hardworking of Chinese Professors and students unstoppably, and now I know the secret of such unprecedented growth. Being a foreigner, I faced many hurdles in my studies due to the language barrier, a real issue for everyone with a different language background. But the one person to whom I will be forever grateful is my co-supervisor, Associate Professor Xudong Yu, the person who has an outstanding theoretical and experimental background. I don't think someone will supervise me better than him. Whenever I encountered any problem regarding my studies or administrative matters in the institute or related to the international school, Xudong Yu was the only person I felt easy to discuss my concerns with. And his guidance, smiley face, and always welcoming personality will be remembered for a lifetime.

The next person I would like to thank is Dr Sadiq Nawaz Khan, and I feel lucky to have him as my friend and mentor. He was the only person who guided me from the very beginning when I started applying to Shanxi University. The day I arrived in Taiyuan, he received me at the airport and guided me about our experimental platform. The different techniques and guidance given by him are unforgettable. At the start of my practical work, it was challenging for me to understand the underlying concept of apparatus, but my seniors helped me a lot. I thank Dr Yuanbin Jin, now a post-doctorate in Purdue University America, for his guidance and support. He always encouraged me to ask questions and his answers were always satisfactory. The next person who has a key role in my studies is my friend and senior Jiangwei Yan. We both faced ups and downs during our studies but always came up with a solution. He taught me a lot of experimental tactics, which benefited me and made me courageous to try different techniques in the experimental platform. I would also like to thank my classmates Miao Jie, Liu Fangde, Nie Liang, Wang Xing Yu for the help offered to me during course work and after that. I

Acknowledgments

would also like to thank Professor Wei Han, Professor Lianghai Huang, Associate Professor Meng Zengming, Associate Professor Liangchao Chen, Professor Wang Pungjun, and specially teacher Qu. Furthermore, I would like to thank my other lab fellows Yan Wang, Chenli Gao, Mi Chengdong, Dr Wen Kai (coldKevin), Dr Li Donghao (now became a teacher in our institute), Yang Guangyu, Shi Zhenlian, Wang Jiangwei, Zhou Fang, Bian Guoqi, Zhang Yue, Li Yunda and all the young guys. I am also thankful to the Chinese scholarship council for funding my study and the international student's office at Shanxi University (Miss Liyan, Meiga and the other teachers), who helped me apply for the scholarship and stay in China. In the end, I would like to thank my Pakistani friends Pir Tariq Shah, Muhammad Tufail, Aftab Ahmad, Behzad Hussain, and others who accompanied me during my stay in China.

Shah Jee Rahman

March 2021, Shanxi University.

Personal Profile

Personal Profile

Name: Shah Jee Rahman
Gender: Male
Race: Utamkhel (Pakhtun)
Native place: Village matako, Distt. Bajaur, Khyber Pakhtunkhwa, Pakistan.
Degree duration: September 2019-July 2022 (Masters)
Institute of Optoelectronics, Shanxi University, Taiyuan, Shanxi, China
Mobile contact: 18536355450 or +923429386605
Email: shahjeekhan018@gmail.com


Previous education:

2013-2015 Bachelor in Physics, Mathematics and Computer science,
University of Malakand, KPK, Pakistan

2015-2017 Master in Physics (two years), University of Malakand, KPK,
Pakistan

Letter of commitment

本人郑重声明：所提交的学位论文，是在导师指导下独立完成的，学位论文的知识产权属于山西大学。如果今后以其他单位名义发表与在读期间学位论文相关的内容，将承担法律责任。除文中已经注明引用的文献资料外，本学位论文不包括任何其他个人或集体已经发表或撰写过的成果。


作者签名： 

2022 年 05 月 17 日

Authorization statement

本人完全了解山西大学有关保留、使用学位论文的规定，即：学校有权保留并向国家有关机关或机构送交论文的复印件和电子文档，允许论文被查阅和借阅，可以采用影印、缩印或扫描等手段保存、汇编学位论文。同意山西大学可以用不同方式在不同媒体上发表、传播论文的全部或部分内容。

保密的学位论文在解密后遵守此协议。

作者签名： 

导师签名：

2022 年 05 月 17 日